

Growing forced bars determine non-ideal estuary planform

J.R.F.W. Leuven¹, L. Braat¹, W.M. van Dijk¹, T. de Haas¹, E.P. van Onselen¹, B.G. Ruessink¹ and M. G. Kleinans¹

¹ Faculty of Geosciences, Utrecht University, Princetonlaan 8A, 3584 CB, Utrecht, The Netherlands

Key Points:

- Quasi-periodic estuary planforms arise from diversion of flow around forced non-migratory mid-channel bars that causes bank erosion
- Self-formed confinements separate zones in which the estuary is wider and bars are more dynamic
- Confinement spacing scales with bar dimensions and estuary width in experiments and nature

Corresponding author: Jasper R.F.W. Leuven, j.r.f.w.leuven@uu.nl

Abstract

The planform of estuaries is often described with an ideal shape, which exponentially converges in landward direction. We show how growing topographically forced non-migratory bars determine the large-scale estuary planform, which explains the deviations observed in the planform of natural estuaries filled with bars compared to the ideal planform. Experiments were conducted in a 20 m long, 3 m wide tilting flume, the Metronome. From a narrow, converging channel a self-formed estuary developed characterised by multiple channels, braided bars, a meandering ebb channel and an ebb delta. Bars hardly migrated due to the alternating current, but the bar width increased with increasing estuary width. At locations where the estuary width was narrow, major channel confluences were present, while the zones between the confluences were characterised by a higher braiding index, periodically migrating channels and a relatively large estuary width. At the seaward boundary, confluences were forced in place by the presence of the ebb-tidal delta. Between confluences, bars were topographically forced to be non-migratory. Diversion of flow around forced mid-channel bars caused bank erosion. This resulted in a planform shape with a quasi-periodic widening and narrowing at the scale of forced bars. Observations in natural systems show that major confluence locations can also be caused by inherited geology and human engineering, but otherwise the estuary outline is similarly affected by tidal bars. These observations provide a framework for understanding the evolution of tidal bar patterns and the planform shape of the estuary, which has wide implications for navigation, dredging and ecology.

1 Introduction

Estuaries are tidal systems that occur where rivers debouch into the sea. The planform of estuaries is often described by an ideal shape [Pillsbury, 1956; Langbein, 1963; Savenije, 2015], which is defined as an equilibrium state wherein the channel planform converges with a constant along-channel tidal range, average depth and current velocity amplitude. The imposed landward-decrease in tidal prism has a first-order control on the planform shape, resulting in converging ("funnel-shaped") channels for delta branches and tidal creeks. However, previous research showed that in alluvial estuaries a second-order complexity is superimposed on the converging shape, which results in more irregular planforms with locally widened zones [Leuven *et al.*, 2018a] (Figure 1). Deviations from the ideal shape may occur because the estuary adapted in varying degrees to its equilibrium shape, depending on the time and sediment available to adapt to changing boundary conditions, such as Holocene sea-level rise and antecedent topography [Townend, 2012; de Haas *et al.*, 2017]. In addition, the outline may be shaped by external restrictions that impose local confinements, such as inherited geology or human engineering, as well as self-formed restrictions, such as salt marshes and riparian forest [Townend, 2012] (Figure 1). Current theoretical and empirical descriptions for estuary planforms neglect the effect that bar formation and bar evolution may have on the planform of the estuary. We propose that the irregular planform of many alluvial estuaries is shaped by a forcing mechanism in which growing mid-channel bars determine bank erosion, leading to quasi-periodic widening and narrowing of the estuary.

In contrast to tidal systems, the forcing mechanism of bars has been thoroughly studied for river systems. Bars can be described as either free or forced, where forced bars are forced to their location by the channel planform shape, while free bars can migrate freely and typically occur in straight or weakly curved channels [e.g. Tubino *et al.*, 1999; Seminara, 2010; Schuurman *et al.*, 2013]. For rivers, low-amplitude alternate bars may cause channel curvature, after which the alternate bars evolve into point bars, forcing a meandering planform [Schuurman *et al.*, 2016].

A recently identified mechanism of coupling between meander and bar formation and bank erosion in rivers [e.g. Parker *et al.*, 2011; Eke, 2014; van de Lageweg *et al.*, 2014] may also be relevant for their tidal counterparts. In the *bank pull* condition, outer-bend bank erosion causes local flow deceleration resulting in inner bend bar growth, while in *bar push* inner bend



52 **Figure 1.** Aerial photographs of (a) Whitehaven beach (Aus), (b) Rodds Bay (Aus), and (c) Netarts estuary
 53 (USA). The outline of these estuaries shows an irregular rather than ideal converging shape. Local
 54 confinements occur due to externally imposed restrictions, such as bedrock geology and human engineering,
 55 as well as by self-formed restrictions. The major confluences occur at locations of confinement. Google
 56 Earth, accessed January-April 2017.

68 sedimentation causes transfer of flow momentum to the outer-bend, which increases bank
69 erosion. Modelling suggests that well-developed bends fluctuate around a balanced state of bar
70 push and bank pull [Eke, 2014], but initially the alternate bars form in a straight channel [van
71 Dijk et al., 2012] suggesting that the process of pattern formation starts with bar push. While
72 this concept has not been applied in estuarine context, the presence of bars and bends suggests
73 that it plays a similar role in estuarine shape and size development. Once variations in width are
74 present, the location and size of forced bars may be induced by channel width variation, for
75 example due to the presence of embayments [Leopold and Wolman, 1960; Yalin, 1971;
76 Struiksmá et al., 1985; Tubino et al., 1999; Repetto and Tubino, 2001; Seminara, 2010; Wu et al.,
77 2011; Kleinhans and van den Berg, 2011; Schuurman et al., 2013]. This suggests an intimate
78 link between bars and river planforms, and we hypothesise a similar dependency between tidal
79 bars and estuary planforms.

80 Indeed, observations in modern estuaries support the hypothesis that the location where tidal
81 bars occur correlates with by the deviation of the estuary planform from an ideal shape [Leuven
82 et al., 2018a,b,c]. In addition, bar and meander dimensions scale with estuary width [e.g.
83 Dalrymple and Rhodes, 1995; Leuven et al., 2016]. From aerial photographs one can observe
84 that the locations where the estuary is relatively narrow correspond to locations with major
85 confluences, defined as the location where two (or more) major channels connect (Figure 1). For
86 braided rivers, the dimensions and spacing of confluences scale with bar dimensions [Ashmore,
87 2001; Hundey and Ashmore, 2009]. Confluence locations associated to downstream bifurcations
88 steer the morphodynamics of channels and bars [Schuurman and Kleinhans, 2015]. For example,
89 the deposition of a mid-channel bar downstream of a confluence location can create a
90 bifurcation and subsequently erode the channel banks, creating a more irregular planform
91 [Hundey and Ashmore, 2009; Schuurman and Kleinhans, 2015]. Here, we explore the relation
92 between channel and bars dynamics and estuary planform. In particular, we assess whether
93 channel and bar dynamics can cause the often observed irregular estuary planform and the
94 locations of major channel confluences.

95 Current knowledge on long-term evolution – time-scales larger than decades – of bars and
96 channels in estuaries is limited by a lack of data [de Haas et al., 2017]. This is mainly due to
97 the fact that observations in modern systems are hampered by the time scale for morphological
98 evolution, which is much longer compared to fluvial systems. In our previous work, we studied
99 present-day bar patterns in natural systems [Leuven et al., 2016, 2018a,b]. Here we shift focus to
100 the morphodynamics of channels and bars. Physical scale-experiments and numerical models
101 complement observations in natural systems because they can provide higher temporal
102 resolution, enabling detailed observation of the morphodynamic evolution of bars. In this study
103 we use physical experiments, because the produced channel and bar patterns in numerical
104 models [e.g. van der Wegen and Roelvink, 2012; Braat et al., 2017] depend on calibration
105 parameters such as the transverse bed slope effect that strongly affect channel-shoal interaction
106 and bar dynamics [Baar et al., 2018; Schuurman et al., 2018].

107 **2 Methods and materials**

108 **2.1 Experimental set-up and procedure**

109 We use a periodically tilting flume of 20 m by 3 m, called the Metronome (Figure 2), that
110 generates dynamic tidal morphology. It produces hydrodynamic conditions capable of
111 transporting sediment during both the ebb and flood phase [Kleinhans et al., 2015a, 2017a],
112 which is uniquely different from earlier physical experiments of tidal systems that relied on
113 periodic sea-level variations [Reynolds, 1887, 1889; Mayor-Mora, 1977; Tambroni et al., 2005;
114 Stefanon et al., 2010; Vlaswinkel and Cantelli, 2011]. The down-scaled magnitude of the water
115 level variations in experiments with periodic sea-level variations, while large relative to water
116 depth, is too low to induce landward sediment transport due to the unscaled grain size.
117 Therefore, previous experiments with periodic sea-level variation resulted in systems with
118 mainly ebb-related transport [Kleinhans et al., 2014]. To obtain similar sediment mobility, scaled

119 estuary experiments with natural sand would require a much steeper bed gradient than natural
120 systems, because of their smaller water depth and bed shear stress, which we obtain by tilting
121 the flume [Kleinhans *et al.*, 2014, 2015a]. The tilting flume allows us to characterize the
122 spatio-temporal patterns of channel and bar evolution. For a more detailed description of the
123 design and hydrodynamics of the Metronome see Kleinhans *et al.* [2017a].

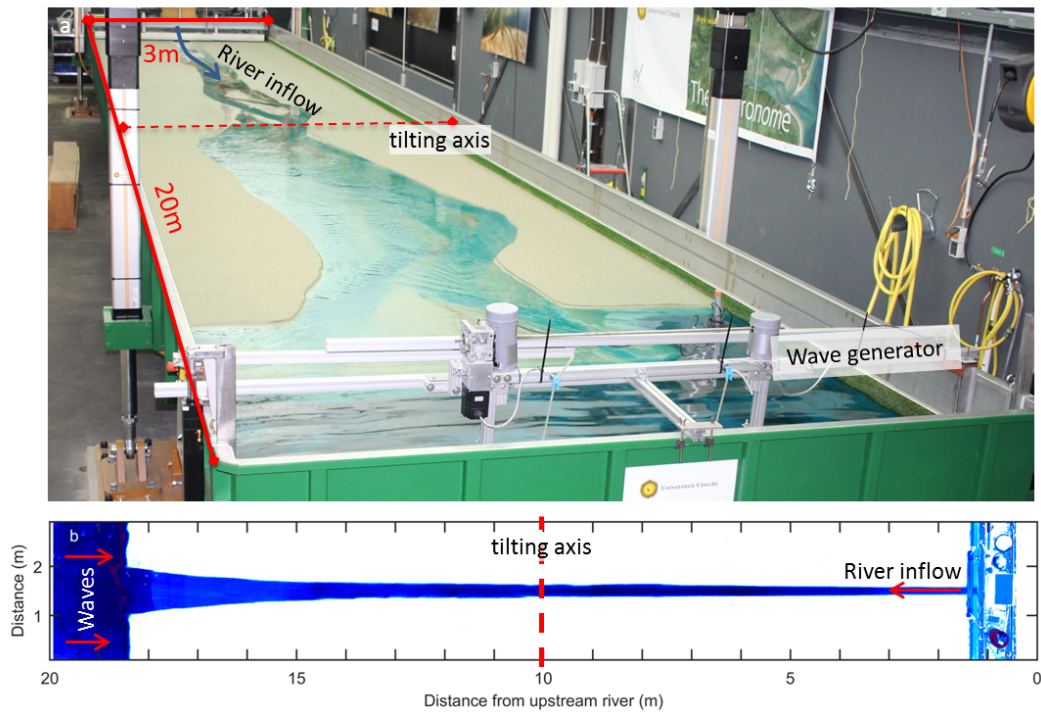
128 Here, we describe one of the experiments with detailed monitoring of the bed elevation and
129 flow velocities and study the long-term evolution of channels and bars. The experiment was run
130 for 15000 tidal cycles, which corresponds to approximately 20 years of natural tidal cycles
131 assuming a semi-diurnal tide. The experimental settings were selected based on a set of
132 approximately 30 pilot experiments in which boundary conditions have been varied
133 systematically, which are reported in the supplementary material of Braat *et al.* [2018]. It was
134 tested whether the settings were such that sediment was well above threshold for motion and
135 that the tidal excursion length, which is the distance a water particle travels in half a tidal cycle,
136 was shorter than the flume length.

137 A plane bed of 0.07 m thick sediment was installed on top of a mat with artificial grass in the
138 basin. Sediment consisted of a sand mixture ($\rho_s = 2650 \text{ kg}\cdot\text{m}^{-3}$) with a median grain size of
139 0.52 mm and a coarse tail ($D_{90}=1.2 \text{ mm}$, $D_{10}=0.33 \text{ mm}$) (Supplementary Figure 1). This
140 sediment mixture was selected to prevent the occurrence of scour holes as much as possible
141 [Kleinhans *et al.*, 2017b]. Another set of experiments were conducted with the addition of
142 crushed walnut shell to simulate the effect of cohesive material, which are reported in [Braat
143 *et al.*, 2018]. We will summarise the effect of this as far as relevant for bar growth and estuary
144 widening in the discussion. The bed was approximately 18 m long and 3.0 m wide. An initial
145 channel was carved in the sediment bed to facilitate the initial flow from the upstream boundary
146 to the sea and back. This initial channel was 0.03 m deep and the width increased exponentially
147 from 0.2 m at the river to 1.0 m at the seaward boundary (Figure 2b).

148 Tidal currents were produced by four actuators that ensured a repeatable tilting with a period of
149 40 s and a maximum tilting gradient of $0.008 \text{ m}\cdot\text{m}^{-1}$. At the upstream boundary water
150 discharge was added to the flume during the ebb phase at a constant rate of $0.1 \text{ L}\cdot\text{s}^{-1}$. River
151 discharge was disabled during the flood phase, because otherwise water would pile up at the
152 upstream boundary, resulting in an extreme water pulse when tilted seaward again. The
153 contribution of the river discharge to the tidal prism is 0.002 m^3 ($0.1 \text{ L}\cdot\text{s}^{-1}\times 20 \text{ s}$), while the
154 total tidal prism is about 0.11 m^3 at the start of the experiment and 0.3 m^3 at the end of the
155 experiment [Braat *et al.*, 2018]. This means that the relative contribution of river discharge to
156 the tidal prism is 1.8% at the start and 0.7% at the end of the experiment. This is within the
157 range that typically occurs in estuaries, e.g. between 0.01% and 20% for estuaries in the UK,
158 with an average of 3% and a median of 0.7% [Manning, 2007].

159 The water level at the boundary between the sea and the land was kept at a fixed elevation by a
160 constant head at the downstream boundary of the flume, allowing free in- and outflow of water.
161 Water depth in the sea was continuously compensated during the tilting by periodic vertical
162 motion of the weir at the seaward boundary, such that the water depth in the sea was always
163 $0.065 \pm 0.005 \text{ m}$ [Kleinhans *et al.*, 2017a]. The water was dyed blue with Brilliant Blue FCF
164 colourant to enhance the visualisation of morphology.

165 Paddle-generated waves were introduced at the seaward boundary with a frequency of 2 Hz and
166 an amplitude of approximately 1 cm during the flood phase. Waves were only introduced during
167 the flood phase, because only in that phase the stirring of sand by the waves would cause slight
168 sediment transport in landward direction. Scale-effects of gravity waves in the Metronome tidal
169 facility are described in the Supplementary Material, but our general conclusion is that the
170 wave-induced sediment mobility is much lower than in natural systems even though the relative
171 wave height with respect to shoreface and channel depth is much larger. Nevertheless, waves in
172 combination with the tidal currents were found to subdue the delta height and the tendency to
173 form large, irregular deltas dominated by channel avulsion.



124 **Figure 2.** (a) The Metronome, a tilting flume of 20 m long by 3 m wide. (b) Overhead image of initial
 125 converging channel bathymetry. Blueness indicates depth, except in the first meter where the gantry is located.
 126 At the landward side, river discharge ($0.1 \text{ L} \cdot \text{s}^{-1}$) was added during the ebb phase. At the seaward end,
 127 paddle-generated waves were applied during the flood phase.

174 Pilot experiments showed that tilting with a simple sine function result in net exporting systems
175 (Supplementary material *Braat et al.* [2018], which means that the system could be classified as
176 a delta sensu *Dalrymple et al.* [1992]. However, we here refer to the system as an estuary,
177 because the relative contribution of river discharge to the tidal volume is too low ($\approx 1\%$) while
178 ebb and flood currents are much larger and approximately equal [*Kleinhans et al.*, 2017a].
179 Furthermore, the observed channels and bars in experiments resemble bars in natural estuaries
180 [*Leuven et al.*, 2016]. Such bars are expected to form much faster than the entire estuary attains
181 equilibrium with its forcing conditions, because bar building only requires lateral sediment
182 displacement over short distances while estuary deformation requires displacement of sediment
183 volumes through the entire system [*Lanzoni and Seminara*, 2006; *Kleinhans et al.*, 2015a]. We
184 therefore argue that the main conclusions in this paper are not sensitive to this simplification.

185 **2.2 Data collection and data processing**

186 Time-lapse imagery from seven overhead cameras was collected each tidal cycle at the
187 horizontal position of the flume when transitioning from ebb to flood flow. The cameras were
188 mounted at equal distances 3.7 m above the centreline of the flume. The CMOS MAKO colour
189 cameras have a resolution of 2048 by 2048 pixels with lenses of a fixed focal length of
190 12.5 mm. The resulting spatial pixel resolution was 1.5-2 mm. Images were geometrically
191 rectified and a lens correction (vignette and distortion) was applied before they were stitched,
192 and then converted to LAB (CIELAB) colourspace images, in which *L* represents the colour
193 band with light intensity, *A* represents red to green and *B* yellow to blue [also used in *van Dijk*
194 *et al.*, 2013]. The *B*-band was extracted from the LAB images, because it enhances the
195 visualisation of morphology by the largest contrast between coloured water and sediment.

196 The flume was illuminated at about 300 lux with daylight-coloured fluorescent light aimed
197 upward at a white diffusive ceiling at approximately 4.5 m above the flume floor. Light
198 reflection from the water surface on the photographs was minimised by white photography
199 backdrop cloth between the ceiling and flume.

200 To create Digital Elevation Models (DEMs), photographs were taken with a digital single-lens
201 reflex (DSLR) camera on a dry bed and processed with structure from motion software [*Lane*
202 *et al.*, 1993; *Chandler et al.*, 2001; *Westoby et al.*, 2012; *Fonstad et al.*, 2013; *Morgan et al.*,
203 2017; *Agisoft*, 2017]. Drainage of the flume, prior to data collection, was slow enough to
204 prevent modification of the morphology. The first 5 DEMs were made with an interval of 500
205 tidal cycles, starting at 300 cycles. Subsequently, seven DEMs were made with an interval of
206 1000 cycles and the final three had an interval of 2000 cycles. The DEMs were referenced with
207 20 ground control points at equal spacing on the sides of the flume, such that the resulting
208 DEMs could be resampled on the same grid as the stitched images from the overhead cameras.

209 Flow velocities were measured over a tidal cycle with Particle Imaging Velocimetry (PIV) [*Mori*
210 *and Chang*, 2003] at 12 moments during the experiment. These 12 moments correspond with
211 the timing of the first 12 DEMs. White floating particles (diameter ca. 2.5 mm) were seeded on
212 the water surface and resupplied when necessary. At 16 equally spaced phases of the tide, ten
213 images were collected with the overhead cameras at 25 Hz, using a pulse train from a frequency
214 generator. Flow velocities were subsequently calculated from pairs of consecutive images with
215 the MPIV toolbox in Matlab [*Mori and Chang*, 2003]. As in *Kleinhans et al.* [2017a], we used
216 the peak cross-correlation algorithm to determine mean particle displacement in pixels in a
217 50x50 window with 50% overlap. The resulting vector fields were scaled to metrics with the
218 pixel footprint of the cameras (1.5-2 mm per pixel), correcting for the tilt of the flume.
219 Erroneous vectors were obtained and filtered out where particles were sparse or overly-abundant,
220 as well as when the PIV-window partly covered the flume wall or reflection on the water surface
221 was too large. For processing, the average vector field was calculated for each tidal phase from
222 ten consecutive images and for plotting purposes it was interpolated on a grid with the same
223 size and resolution as used for the overhead cameras and DEMs. Residual currents were
224 calculated as the average flow vector over a full tidal cycle.

2.3 Data reduction

Experimental results are compared with data from natural systems [Leuven *et al.*, 2016] to assess how well the tidal bars in our experiment scale to nature. A detailed comparison is made with the Western Scheldt (NL), for which detailed bathymetries over time and flow velocities are available. In this study, the important scaling properties are the planform dimensions of bars and the elevation distribution of the bathymetry. Therefore, maximum bar length and width were measured in the experiments following Leuven *et al.* [2016]. Hypsometric curves, which are cumulative depth elevation curves, were calculated for four zones in the experiment as well as for the Western Scheldt. These zones were chosen as the part between two successive width confinements in the estuary (Figure 3k, Supplementary Figure 6a).

Estuary width was measured in our experiment as the local width between the non-eroded estuary banks. Channel width was measured as the width of the estuary below an along-channel linear profile that was fitted on the median bed level per cross-section, whereas above the median bed level was classified as bar. Excess width is defined as the estuary width minus the width from an ideal converging estuary shape and summed width of bars was measured as the sum of the width of all bars in a cross-section [Leuven *et al.*, 2018a].

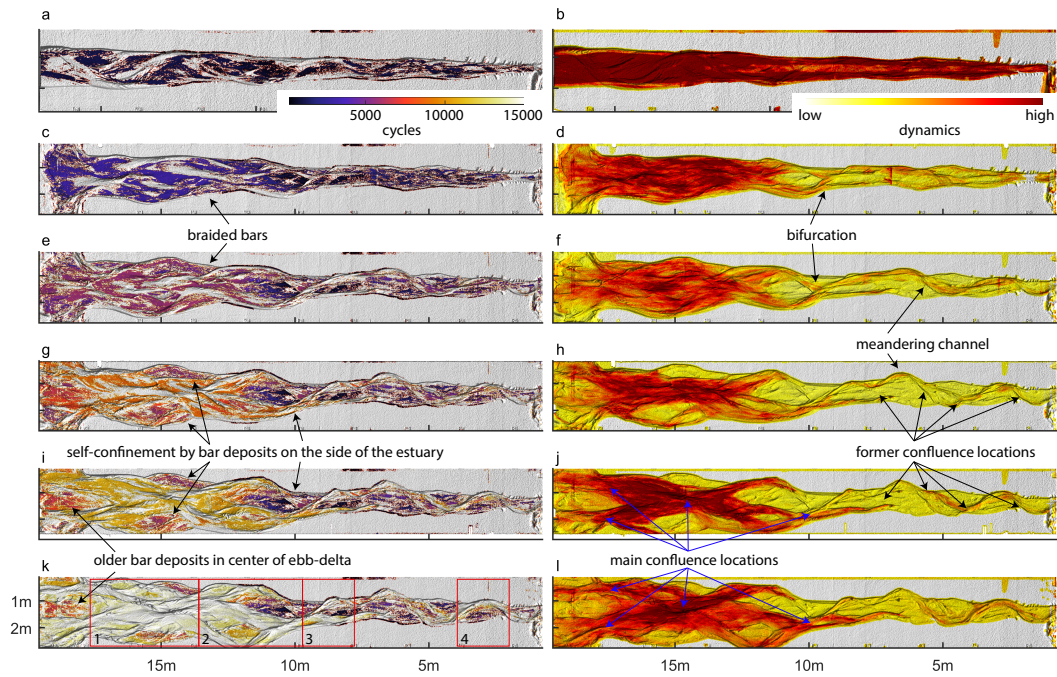
The locations of major channel confluences and the spacing between them over time were determined for the experiment and the Western Scheldt. In addition, these quantities were measured on aerial imagery for a fixed moment in time in 7 other natural systems: Dovey (UK), Bannow (UK), TawTorrige (UK), Teign (UK), Rodds Bay (Australia), Whitehaven beach (Australia) and Netarts (USA). In case of aerial photographs, major confluence locations were visually determined as the deepest point where multiple channels converge, while these points were extracted from bathymetric data for the experiments and Western Scheldt (Figure 4). Deep scours as a result of bank protection, resistant layers that consist of shell fragments (so called 'craggs', Cleveringa [2013]), or scours associated with outer bends of meanders were excluded. Subsequently, the location and spacing between successive channel confluences were measured with respect to local zones of confinement in the estuary outlines.

The dynamics of channels and bars over time were studied from the blueness images, which is a proxy for the water depth. Blue represents the channel and white the bar. Changes in blueness values were used to study where erosion and sedimentation occurred in the experiment and to determine the youngest time step during which sediment was deposited. The same approach was applied using successive DEMs of the experiment, but the temporal resolution for this was lower. Cumulative bed level change was calculated as a measure of the spatial dynamics within the system and to assess whether the experiment was in dynamic equilibrium during the final stages. Cross-sectional profiles were taken from the LAB images and plotted over time, creating time-stack diagrams that show the migration of channels and bars in cross-section over time.

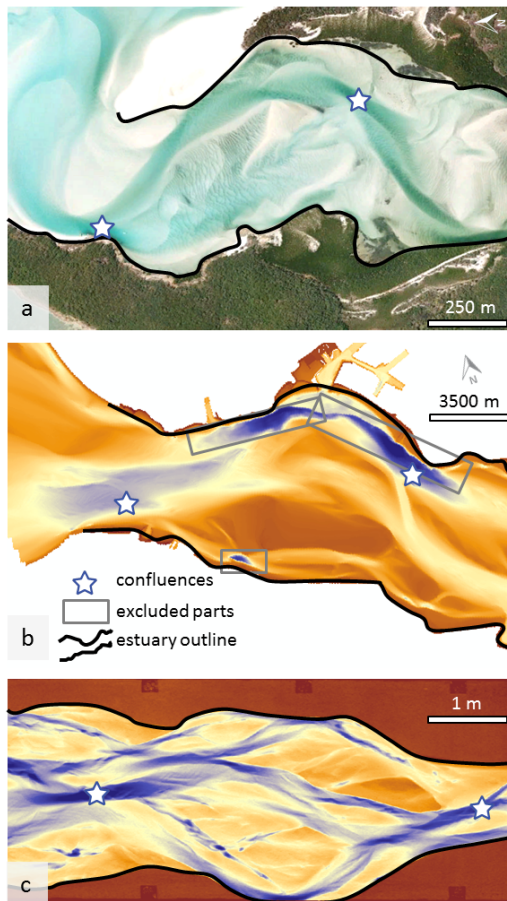
3 Results

3.1 General morphological evolution

In the initial phase of the experiment, an alternate bar pattern evolved (Figure 5a). As channel widening continued, a main meandering channel formed with riffles between two successive bends. The meandering channel and alternate bars initially migrated seaward (Supplementary Movie). Later, the increased curvature of the meandering channel forced the bars (i.e. they became non-migratory) to their inner bends, while lateral erosion and deposition increased the width of the forced bars. In a later stage, channels stabilised in the landward part of the estuary, while the estuary width kept increasing in the seaward part. This allowed the development of multiple bars and channels in cross-section, which were first observed when flood 'barbs' intersected the forced bars (Figure 5a,b). Barb channels are channels that become shallower in the direction of flow and have a dead end on the bar. Net sediment transport towards the sea formed an ebb-tidal delta, which is a term more commonly used in the context of tidal basins but also applies to estuaries [e.g. Davis Jr and Hayes, 1984; Elias *et al.*, 2017]. The ebb-tidal



235 **Figure 3.** Two representations of spatiotemporal patterns of morphodynamics. [left] Hillshade map of
 236 morphology at several time steps, showing increasing age variation as the system develops (top to bottom).
 237 The colour scale indicates time of deposition of the top surface, where light colours are the youngest. [right]
 238 Hillshade map of morphology at several time steps, in which the colour scale indicates cumulative bed level
 239 change between two successive DEMs, which is an indicator of dynamic activity. Maps are given for the
 240 following time steps: (a,b) 1250, (c,d) 3300, (e,f) 5900, (g,h) 8900, (i,j) 10900 and (k,l) 15000 cycles. Red
 241 numbered boxes in (k) show the zones for which hypsometric curves are calculated (Figure 10c).



259 **Figure 4.** Locations of major confluences were determined in (a) aerial photographs of natural systems, (b)
 260 bathymetry of the Western Scheldt and (c) and experiments. Warm colours denote high elevation, cool
 261 colours denote low elevation. In case of aerial photographs, major confluence locations were chosen where
 262 multiple main channels converge. For the bathymetry of the Western Scheldt and experiment, these points
 263 were automatically determined as the maximum depth within a confluence zone. Deep scours as a result of
 264 bank protection, presence of hard layers or outer-bend erosion were excluded.

288 delta limited the inflow of water to the estuary. As widening progressed, forced mid-channel
 289 bars diverted the flow and periodically caused bank erosion. These zones were alternated by
 290 locations where the estuary width remained narrow or was self-confined by sidebar deposits,
 291 resulting in a quasi-periodic planform (Figure 5d,e).

294 **3.2 Channel widening and incipient meandering**

295 The initial phase of the experiment was characterised by the development of the initial
 296 converging channel into an incipient meandering ebb-tidal channel (Figure 5a). In the first 200
 297 cycles, the converging straight channel widened (Figure 6) and initially free (seaward migrating)
 298 alternate bars formed. The resulting channel pattern consisted of multiple straight channels
 299 parallel to the centreline of the estuary, which were separated by sills that connected the
 300 alternate bars in along-channel direction. Over time, the straight channels became more oblique
 301 to the estuary centreline and curved until they developed a meandering ebb-tidal channel, which
 302 forced the bars in place. On top of the alternate bars, circulating flow patterns developed, with
 303 residual currents dominantly moving in landward direction onto the bars, then diverting to the
 304 channel and flowing back in seaward direction via the meandering channel (Figure 7a). Both the
 305 ebb and flood flows caused erosion of the estuary banks by lateral migration of channels in the
 306 following tidal cycles (Figure 7b).

317 **3.3 Alternate bars with initial barb formation**

318 This phase was characterised by the formation of barb channels in the inner bends of the
 319 alternate bars. The main meandering ebb channel migrated laterally eroding the estuary banks
 320 and alternate bars grew in width. At the landward side shallow sills formed between two
 321 successive alternate bars. The sill separated the ebb flow from the flood flow in two separate
 322 channels. As the ebb channel migrated further seaward and the flood channel landward,
 323 u-shaped bars formed (Figure 5a). The u-shaped bars thereby partly blocked the channel with
 324 opposing flow (Figure 5a).

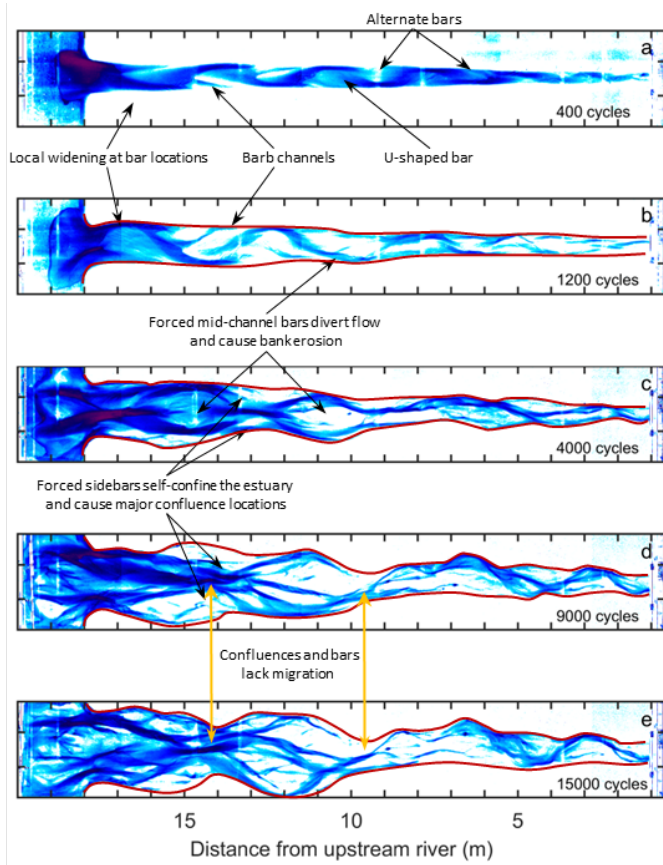
325 From 1000 tidal cycles onward the braiding index, which is the average number of channels or
 326 bars in the cross-section, kept increasing as a result of the increasing channel width, which
 327 allowed for multiple braided bars (Figure 5a). Bars were particularly abundant in specific zones
 328 (at approximately 8 m, 11 m, 14 m and 15 m) where the summed width of bars was large
 329 (Figure 8a,b) and the compound bars were dissected by one or multiple barb channels.
 330 Compound bars are more complex bars that probably amalgamated from other bars, in analogy
 331 with rivers [e.g. *Bridge*, 2003; *Ashworth et al.*, 2000; *Schuurman et al.*, 2013].

340 At the seaward side, the export of sediment during the first 2000 cycles formed an ebb-tidal
 341 delta. After this period, the delta was large enough to limit the inflow of water into the estuary,
 342 while erosion on the delta formed a single major channel at the northern side of the inlet
 343 (Supplementary Figure 2h,i).

344 The location of the main meandering channel shifted from north at 1000 cycles, to south around
 345 2000 cycles and back north at about 3000 cycles at approximately 15 m from the upstream
 346 boundary (Supplementary Figure 2e,h,i). Interestingly, the adjacent channel confluence positions
 347 (at 13.5 m and at the mouth of the estuary) were relative stable over time, with dynamic bar and
 348 channel zones in between. This caused a rather irregular pattern in the outline of the estuary
 349 where some parts remained relatively narrow while other parts became relatively wide
 350 (Figure 6).

351 **3.4 Mid-channel bars, confluences and evolution of quasi-periodic planform**

352 In the central part of the estuary (8-18 m), widening resulted in the formation of forced
 353 mid-channel bars that diverted flow, which caused bank erosion. For example after 4000 cycles,
 354 a large estuary width at 15 m allowed the existence of two major channels: one on the northern

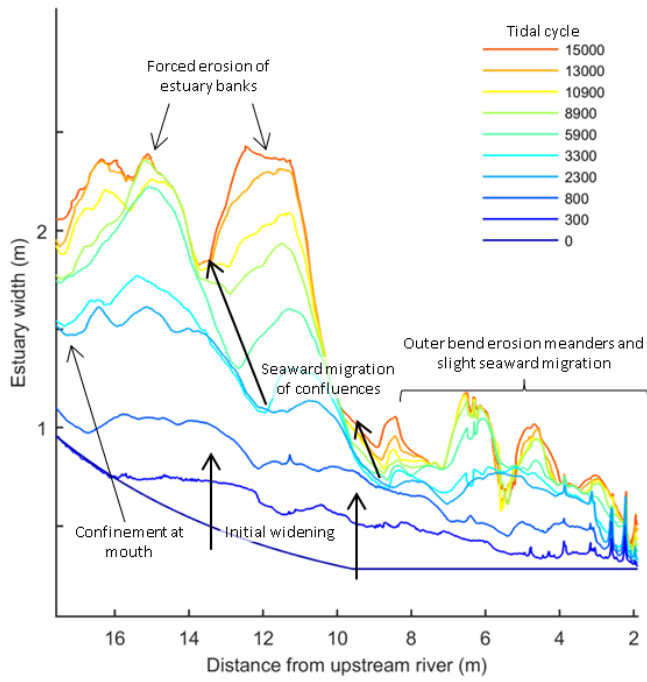


292

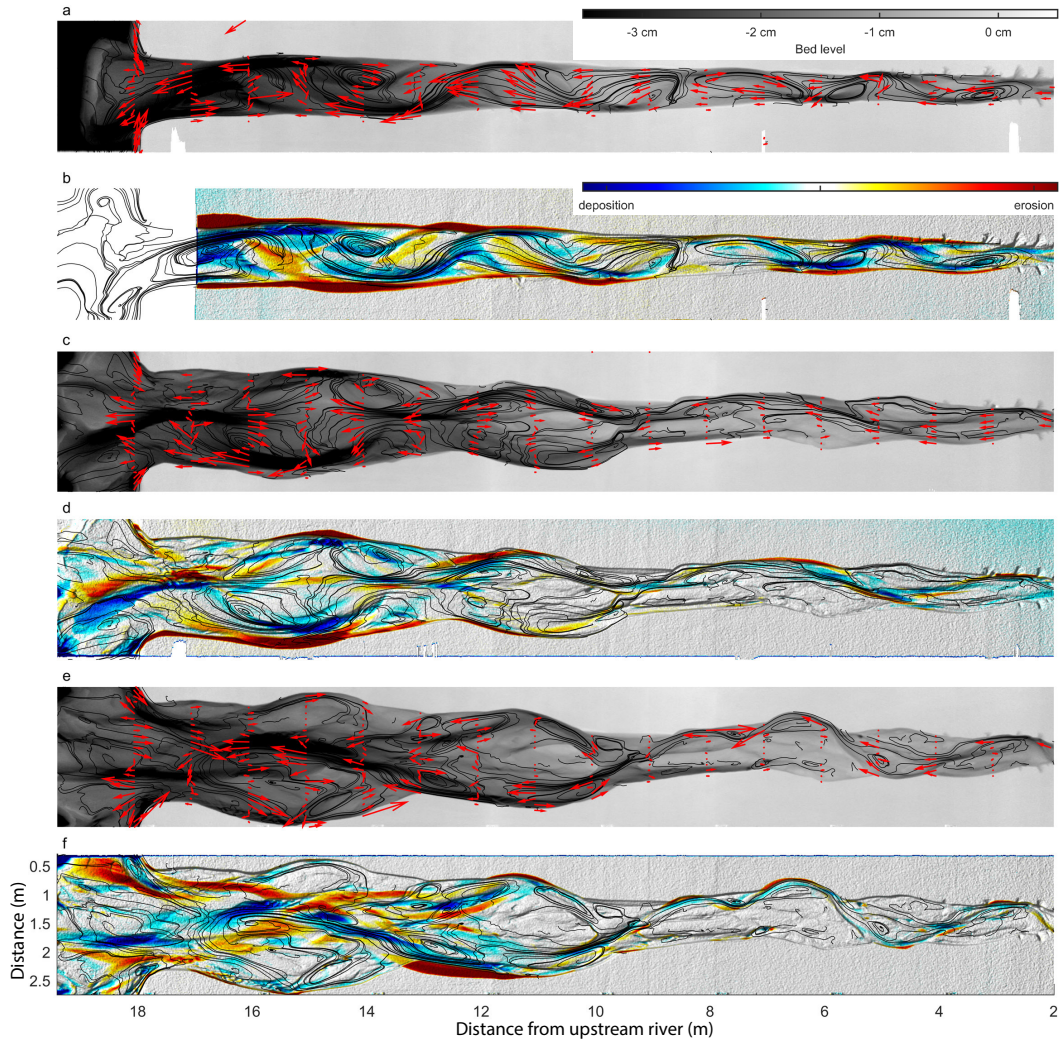
Figure 5. Overhead imagery of the experiment for five moments in time. Blueness was extracted as an

293

indicator for channel depth. For all time-steps, see Supplementary Figure 2 or the Supplementary Movie.

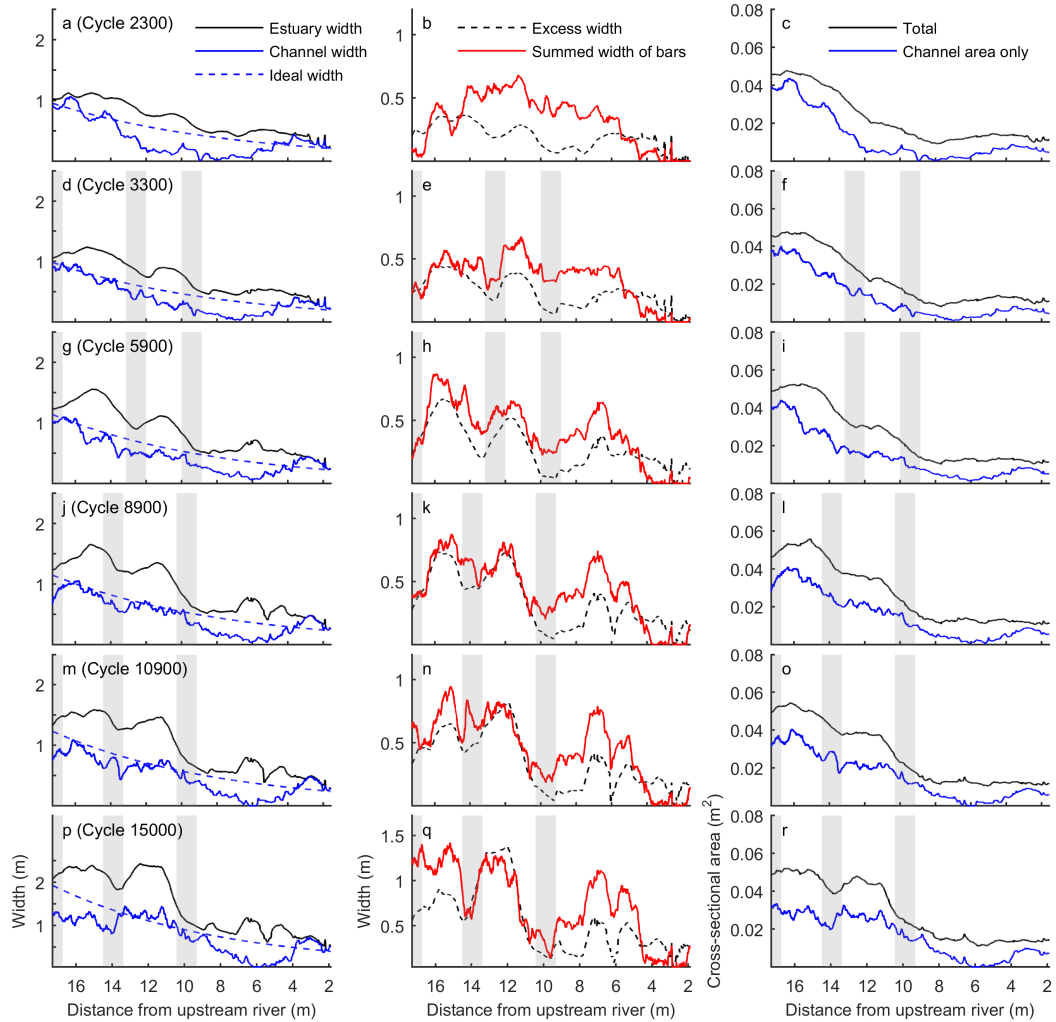


307 **Figure 6.** Evolution of the estuary width profile. The planform initially widened and, from 2300 cycles
 308 onward, became more irregular. After 3300 cycles, bars and landward meanders rapidly force local widening,
 309 while confinements migrate seaward. In the last phase, after 8900 cycles, the bars became static (forced) and
 310 bank erosion ceased at the confluence locations, while the amplitude of the quasi-periodic width variation
 311 increased where mid-channel bars were present.

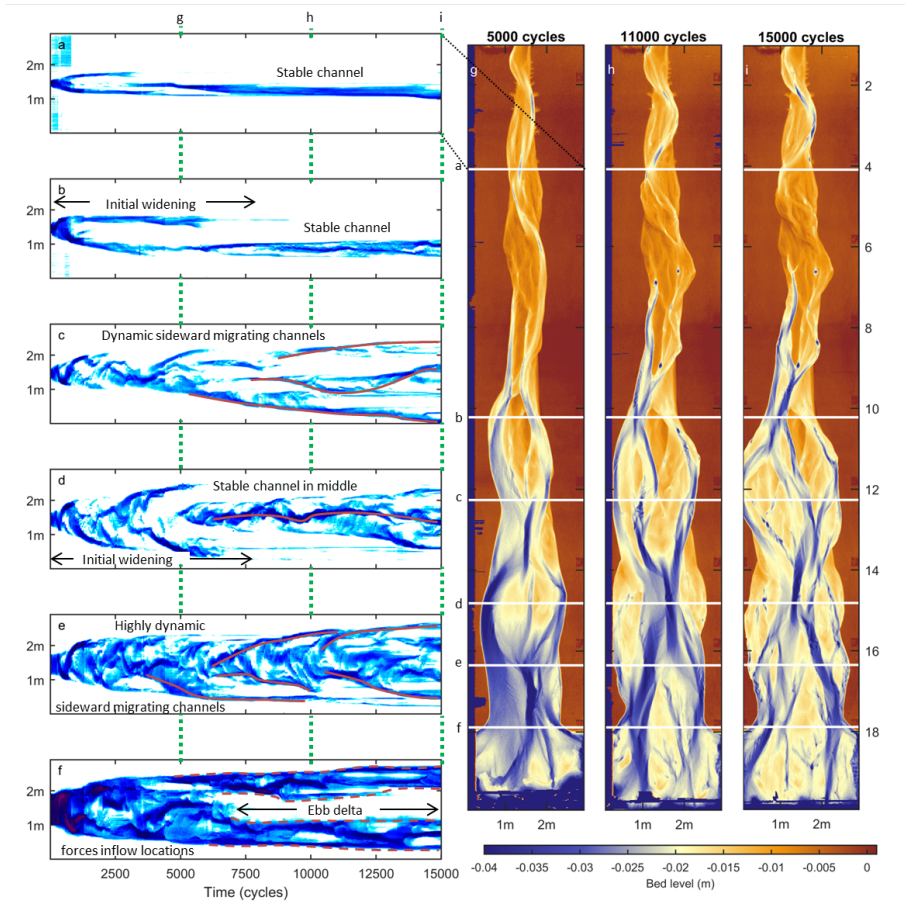


312 **Figure 7.** (a,c,e) Vectors indicating the residual currents after (a) 800, (c) 4400 and (e) 6900 cycles for
 313 transects with a spacing of a meter on top of a map with the streamlines based on a vector field with residual
 314 currents and the bathymetry. (b,d,f) Streamlines based on a vector field with residual currents, plotted on top
 315 of a map that indicates the erosion (in increasing magnitude from yellow to red) and sedimentation (from cyan
 316 to blue) in the subsequent phase of the experiment.

355 side and one on the southern side of the estuary, separated by a relatively wide bar in the centre
 356 of the estuary (Figure 5c). The confluences of these two channels occurred at the mouth of the
 357 estuary and at 13.5 m in a channel located in the middle of the estuary. While the two major
 358 channels at 15 m continued to migrate towards the outer banks of the estuary (Figure 9d), the
 359 bar between these channels obtained an oval shape as a result of an almost symmetrical ebb and
 360 flood barb on both its landward and seaward side. The residual current showed two major
 361 circulation cells at this compound bar (Figure 7c). The flood barb facilitated flow onto the bar,
 362 which diverged over the bar to the channels north and south of the bar. The ebb flow
 363 predominantly used the northern and southern channel around the bar and any flow entering the
 364 ebb barb also diverged into these channels. This caused bank erosion on both the north and
 365 south side of the estuary and sedimentation that increased the width of the mid-channel bar
 366 (Figure 7d). A similar process occurred in a more landward part slightly later in the experiment.



332 **Figure 8.** [left] Evolution of estuary width, channel width and ideal width. [middle] Evolution of excess
 333 width and summed width of bars. [right] Evolution of cross-sectional area. Estuary width is the sum of
 334 channel and bar width. Ideal width is the largest fitting exponential shape in the estuary outline. Excess width
 335 is the estuary width minus the ideal width. The channel width approaches an ideal converging shape over
 336 time. Summed width of bars approaches the excess width. Total cross-sectional area is the area below the
 337 estuary banks. Channel cross-sectional area excludes the area above bars. Shading indicates the locations
 338 where the estuary remained confined. At these locations, the summed channel width and summed bar width
 339 remain relatively low.



367 **Figure 9.** (a-f) Time-space diagrams of cross-sections at 4, 10, 12, 14.5, 16 and 17.5 m, which are
 368 indicated in (g,h,i) bathymetry after 5000, 11000 and 15000 tidal cycles. (a,b) A single landward channel
 369 stabilises from 7500 tidal cycles onwards. (c) In the centre, dynamic, sideward migrating channels occur. (d)
 370 Outward migrating channels erode the estuary banks. From about 6000 cycles the mid-channel bar is
 371 cross-cut and a single main channel forms in the middle of the estuary. (e) In the seaward part, multiple very
 372 dynamic, migrating channels occur. The channels migrate from the estuary centreline towards the estuary
 373 banks. (f) An ebb-tidal delta forms and stabilises after 7500 tidal cycles. This forces the inflow locations to be
 374 on the sides of the ebb-tidal delta.

375 In the landward part of the estuary (0-8 m) the individual channels became more curved and
 376 connected, so that a main meandering channel formed from 5000 cycles onward (Figure 5c,d).
 377 The channel orientation of the upstream channel affected diversion of flow and sediment at the
 378 former bifurcation at 9 m, so that now the landward river system fed the southern branch instead
 379 of the northern branch (Figure 5c,d). This channel subsequently migrated (Figure 9c) by eroding
 380 the southern bank of the estuary at 10 m (Figure 7f), whereas the northern channel was only
 381 connected during flood flow. Seaward, the southern channel merged with the major channel that
 382 formed in the middle of the estuary at approximately 13 m. At this point multiple smaller barb
 383 channels formed onto the bar at 11 m that evaded each other and migrated over the bar.

384 At the mouth, the estuary was slightly narrower than the part of the estuary directly landward of
 385 the mouth at 16 m. Specific zones occurred where estuary width was relatively narrow with a
 386 major confluence and approached its ideal width. The zones were alternated by zones in which
 387 the estuary was much wider (Figure 8). Over time, the confluences migrated slightly seaward
 388 and the planform became progressively less ideal (Figure 6). The landward channel (0-8 m)
 389 eroded the estuary banks in the outer bends of the meanders until approximately 8000 tidal
 390 cycles. From that moment on the configuration of channels and bars in the landward part
 391 (0-8 m) remained relatively stable over time (Figure 5d,e, Figure 9a,b). The later phases of the
 392 experiment (6000-15000 cycles) were characterised by specific zones that were active
 393 (Figure 3h,j,l). These zones connected the major channel confluences at 10 m, 14 m and 18 m.
 394 The active zones were relatively narrow at locations where the confluences occurred (e.g. at
 395 14 m and 18 m in Figure 3j) and relatively wide in the zones in between (e.g. at 16m).

396 **3.5 Cross-cutting of mid-channel bars**

397 In the seaward part, the phase with mid-channel bars and bank erosion continued until 5000
 398 cycles, when a channel was able to progressively cut through the middle of the bar, connecting
 399 the barb channels around 5000-5500 cycles (Figure 5c,d). This caused a main channel along the
 400 centreline of the estuary. During this phase, the major in- and outflow was focused in the
 401 middle of the ebb-tidal delta. This reduced bank erosion in the most downstream part of the
 402 estuary from that moment onward (Figure 6, 14-18 m), preventing the estuary shape from
 403 becoming more irregular.

404 In the central part of the estuary, the cross-cutting event also caused the direction of the residual
 405 circulation cells to reverse, with flood flows now predominantly occurring along the sides of the
 406 estuary, while the channel in the middle of the estuary was ebb dominant (Figure 7e). This
 407 reduced erosion of the estuary banks at this location and triggered the formation of new
 408 channels that connected the main ebb channel with the newly formed outflow locations on the
 409 ebb-tidal delta (Figure 7f). Because the main channels in the middle of the seaward part of the
 410 estuary (14-18 m) gradually exported sediment to the central parts of the ebb-tidal delta, this
 411 process eventually blocked the in- and outflow of water (6000-8000 cycles) (Supplementary
 412 Figure 2n-p). The ebb delta thus stabilised in place after 7500 tidal cycles (Figure 9f,h), after
 413 which the in- and outflow of water became diverted to the northern and southern sides of the
 414 ebb-tidal delta (Figure 9f).

415 Similarly to the previous bar cross-cutting event around 5000 cycles, a similar process occurred
 416 at the compound bar more landward (9.5-13 m), where after 9000 cycles the cross-cutting of the
 417 middle parts of the bar occurred (Figure 5d). This isolated a southern part of the compound bar
 418 at 9.5 m. In short, the estuary evolved from an initially converging channel into an estuary filled
 419 with bars that inherited its quasi-periodic planform from phases in which mid-channel bars
 420 diverted flow laterally, causing bank erosion.

421 **3.6 Progressive infill from the sea and dynamic equilibrium with stable confluences**

422 The zones where the estuary was confined reflect the locations where bars were relatively less
 423 abundant. For natural systems, a correlation was found between the occurrence of tidal bars and

424 locations where the excess width is large [Leuven *et al.*, 2018a], which is defined as the local
 425 estuary width minus the ideal estuary width. This is in agreement with the experimental results
 426 (Figure 8h,k,n), where summed width of bars indeed approaches the excess width in the later
 427 stages of the experiment. While the zones between 4-8 m and 14-18 m deviated from this rule
 428 in magnitude, the along-channel pattern is the same, i.e. low excess width corresponds to low
 429 summed width of bars and vice versa.

430 In the last phase, the estuary reached a dynamic equilibrium with stable confluences, while
 431 active channel migration remained in the parts between the confluences. Mean changes in bed
 432 level and sediment export illustrate that the experiment was close to dynamic equilibrium
 433 (Supplementary Figure 3). Generally, the increase in estuary width that was observed in
 434 previous stages decreased and only in the part 10-13 m and at the mouth of the estuary a slight
 435 increase in width occurred during the last 2000 cycles of the experiment (Figure 6).

436 In the final stages of the experiment, flow from the landward side bifurcated around the newly
 437 isolated bar at 11 m (10000-12000 cycles, Figure 5d,e), after which the northern branch began
 438 to erode the southern side of the former bar between 9.5 m and 12 m. At the same time the
 439 southern branch continued to erode the southern bank of the estuary until reaching the flume
 440 wall, which was the reason to end the experiment after 15000 cycles.

441 **4 Discussion**

442 This study presents the first physical scale-experiment of an estuary with dynamic channels and
 443 bars, stable confluences, and a self-formed planform. Below, we first describe a conceptual
 444 model on how forced bars determine the estuary outline. Second, we discuss the spatial and
 445 temporal scaling of bars. Then, the effect of bar patterns on the flow patterns is compared with
 446 the evolution of natural estuaries. Last, the observed experimental cyclicity in channel and bar
 447 migration is compared to natural systems.

448 **4.1 Conceptual model for estuary planform forcing**

449 We summarise the evolution of a self-formed estuary in a conceptual model containing three
 450 phases. In the first phase (Figure 13a) an alternate bar pattern develops, while the estuary
 451 widens. The initially straight channels connect to form a meandering channel with alternate bars
 452 [comparable to alternate bars in rivers *Struikma et al.*, 1985; *Ikeda and Parker*, 1989; *van de*
 453 *Lageweg et al.*, 2014]. As soon as the bars exceed a width-to-length ratio of approximately 1/7,
 454 the flood flow is capable of forming barb channels onto the alternate bars (Figure 13a). The
 455 barb channels progressively cut through the alternate bars. Both the outer bends of the
 456 meandering channels and the flood barbs erode the estuary banks, which creates an irregular
 457 estuary planform.

458 In the second phase, the first mid-channel bars have formed that are large enough to divert the
 459 flow such that the outer-bend erosion is accelerated and major confluences are formed seaward
 460 and landward of the mid-channel bars forming a quasi-periodic estuary planform (Figure 13b).
 461 At the confluence locations, estuary width generally remains narrow and dynamic channels and
 462 bars only occur within a small stretch of the estuary width. As outer-bend erosion continues, the
 463 gradient over the mid-channel bar becomes favourable for both the ebb and the flood flows.
 464 These flows create new barb channels onto the mid-channel bar, which over time are capable of
 465 cross-cutting the bar, forming a new main channel in the middle of the estuary (Phase III,
 466 Figure 13c). The timing of this event may vary along the estuary and confluences typically
 467 migrate seaward over the course of these phases.

468 After this phase, a dynamic equilibrium at the bar-confluence scale is reached, in which
 469 sediment from bars and banks is reworked into new bars within the estuary. The confluences
 470 remain stable and bank erosion is reduced. Dynamic zones of channels and bars typically occur
 471 in stretches between the major confluences. In both experiments and natural systems we

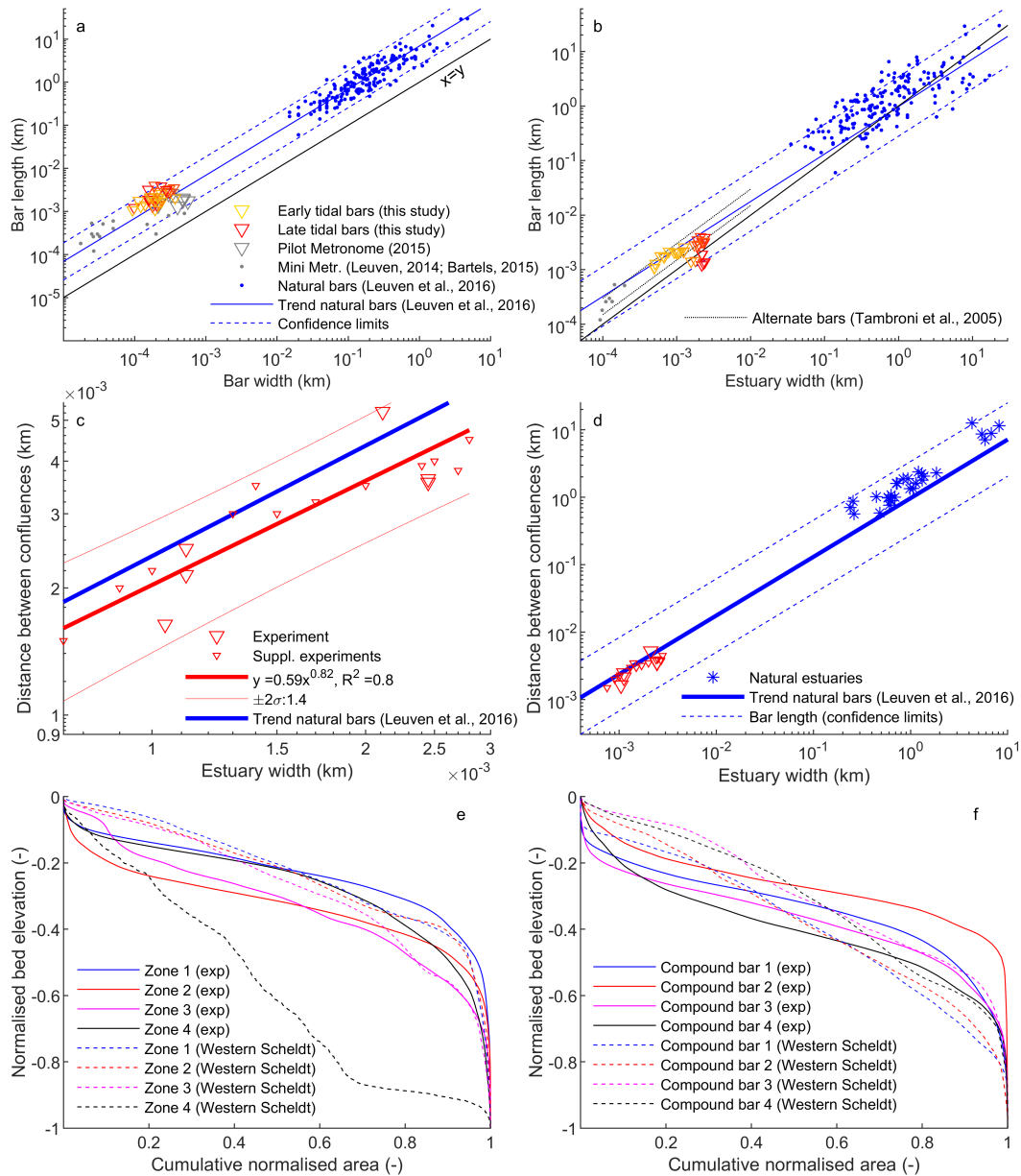
472 observed the development of irregular estuary planforms and the forcing of channel confluences
473 and zones with dynamic channels and bars. The conceptual model implies that quasi-periodic
474 deviations from the ideal estuary shape can be formed autogenically. This means that the
475 planform shape of natural estuaries is not necessarily externally forced, i.e. allogenic, for
476 example by the presence of bedrock or resistant layers.

477 Our observations show that the mechanisms of bar push and bank pull identified in rivers [e.g.
478 *Parker et al.*, 2011; *Eke*, 2014; *van de Lageweg et al.*, 2014] may apply in estuaries as well.
479 Initially, the alternate bars form in a straight channel, which was also the case in river
480 experiments [*van Dijk et al.*, 2012], suggesting that the process of pattern formation starts with
481 bar push. However, in later phases, as soon as the increased curvature and local widening [e.g.
482 *Repetto and Tubino*, 2001; *Seminara*, 2010; *Zolezzi et al.*, 2012] forces the bars to be
483 non-migratory, the usual meander bend migration mechanism of curvature-driven momentum
484 displacement towards the outer bank kicks in, causing bank retreat. This is followed by inner
485 bend accretion, meaning that this phase is dominated by bank pull. Upon further widening, the
486 bar regime shifts to mid-channel bars that are non-migratory because of curvature and local
487 widening as well as the tidal reversing flow, and the process continues on both sides of the bar.
488 We hypothesise that this stage is dominated by a balance between bank pull and bar push as in
489 *Eke* [2014].

490 **4.2 Spatial and temporal scales of channels and bars**

491 The dimensions of tidal bars in the experiments scale well with bars observed in natural
492 systems, as reported in *Leuven et al.* [2016] (Figure 10a). All experimental bars are within the
493 uncertainty margins given for natural bars. However, most experimental bars plot above the
494 trend line, indicating that their shape is slightly more elongated compared to the bars in natural
495 systems (length-to-width ratio of approximately 8 in experiments, compared to 7 in nature).
496 Moreover, the bar length is well within the range as expected based on local estuary width
497 (Figure 10b). The experimental bars have similar dimensions as the alternate bar pattern
498 reported in *Tambroni et al.* [2005] where the average bar wavelength is 3-6 times channel width,
499 thus bar length is 1.5-3 times channel width. However, in contrast with experiments with fixed
500 channel planimetry [*Tambroni et al.*, 2005, 2017] that result in a system with a braiding index of
501 1, we observed rapid widening of the estuary, which allows braiding index, bar width and bar
502 length to increase. Most experimental bars fall exactly on the trend expected from natural
503 systems. The largest outliers occur at the lower uncertainty band. These bars are an order of
504 magnitude smaller than the other bars and formed in later phases of the experiment in one of
505 the larger channel branches in the estuary. In this case, the width of the single branch is
506 responsible for the bar dimensions. Therefore, scaling with the full estuary width may result in
507 large deviations from the expected trend.

520 Hypsometric curves for four zones within the estuary (indicated in Figure 3k and Supplementary
521 Figure 6a) show a large similarity between the experiment and the Western Scheldt
522 (Figure 10e), where zones were defined as the estuary area between two successive
523 confinements. Only zone 4 in the Western Scheldt deviates significantly from the hypsometry in
524 the experiment (Figure 10e). At this location the estuary width is smaller and thus a larger part
525 of the width is influenced by dredging to maintain shipping fairways. When channels are
526 excluded and thus hypsometric curves are drawn for compound bars only, bars in the Western
527 Scheldt show a more linear elevation profile, while bars in the experiment have a more s-shaped
528 curve (Figure 10f). The s-shaped curves for the experiment are caused by a small portion of the
529 compound bars being highly elevated and a small portion being very low elevated. High
530 elevated parts developed on the oldest parts of bars that accreted over time and lack flooding
531 and morphodynamic activity in later phases. The relative scarcity of high elevated areas is
532 caused by the lack of cohesive material and vegetation, which would otherwise accrete tidal bars
533 and estuary banks [*Braat et al.*, 2017, 2018; *Lokhorst et al.*, 2018]. Low elevated parts are
534 previous channels or scours on bars for which time was too short to fill in.



508 **Figure 10.** (a) Comparison of planform bar dimensions (length versus width) in the experiments and in
 509 natural systems. Triangles represent bars in the experiment, with colour indicating the tidal cycle during
 510 which the bars were measured: yellow was early in the experiment, red was at the end. (b) The scaling
 511 relation between estuary width and bar length that was found for natural systems holds for the experiments
 512 [Tambroni et al., 2005; Leuven, 2014; Bartels, 2015]. (c) Confluence spacing as a function of local estuary
 513 width for experiments. Each triangle is the spacing between two successive confluence locations. (d)
 514 Comparison of confluence spacing in experiments with natural systems. A line with predicted bar length
 515 ($\times 1.5$) is drawn for comparison and shows that confluence spacing scales with bar dimensions and estuary
 516 width. (e) Hypsometric curves of zones between two successive confinements in the estuary outline, with
 517 numbering increasing in landward direction. The corresponding zones are given for the experiment in
 518 Figure 3k and for the Western Scheldt in Supplementary Figure 6a. Parts above the high water level were
 519 excluded. (f) Hypsometric curves of compound bars in the same zones.

535 As bars separate the major confluences, it was expected that confluence spacing scales with bar
536 dimensions, which scale with estuary width (bar length \propto channel width^{0.87}, *Leuven et al.*
537 [2016]). Indeed, this was found to be the case (Figure 10c,d), which means that the spacing of
538 confluences scales well with bar dimensions and estuary width. In general, this also implies a
539 decreasing confluence spacing along-channel from the sea in landward direction, because
540 estuary width and bar dimensions decrease. To quantify the location where confluences occur,
541 we measured the distance from the location of the major confluences to the local minima in the
542 outline of the estuary. The measured distance was normalised by the average spacing with the
543 successive landward and seaward confluence locations. Results show that the major confluences
544 in all cases occur within 16% of local confinements for the experiments and Western Scheldt
545 over time, as well as for the aerial photographs of 8 natural systems (Supplementary Figure 4).

546 The timescale over which the channels and bars in the experiment evolve is 15000 tidal cycles,
547 which corresponds to approximately 20 years of natural tidal cycles. All the sediment eroded in
548 the experiment is either used for bar formation or exported to the ebb delta, which is a
549 long-term sink for the eroded sediment for lack of intense littoral processes. Most modern
550 estuaries typically evolved over centuries to millennia during the middle to late Holocene under
551 rising sea level [*van der Spek and Beets*, 1992; *Hijma and Cohen*, 2011; *de Haas et al.*, 2017].
552 As such, their evolution comprised many more tidal cycles than our experimental estuary.
553 Typically, modern estuaries initially enlarged as former river valleys that drowned, because of
554 the rapid sea-level rise around the start of the middle Holocene. Part of the slower evolution
555 may thus be explained by the time required for aggrading after sea-level rise decreased, in
556 contrast to the erosional behaviour in the experiment. The relatively rapid evolution of bar
557 patterns and bank erosion was also observed in river experiments and may partly be explained
558 by a lack of bank strength in experiments without vegetation and cohesive material [*van Dijk*
559 *et al.*, 2012].

560 Additional experiments with added cohesive material [*Braat et al.*, 2018] revealed two major
561 effects compared to the experiment reported in this study. First, the mud fills up inactive areas
562 and predominantly accretes on the tidal bars and estuary banks, which reduced the tidal prism.
563 This counteracts the positive feedback mechanism between estuary widening, increased tidal
564 prism and therefore increased cross-sectional area at the mouth. The second effect is that the
565 cohesiveness of mud has a slight stabilising effect on gentle slopes. However, the cohesion has
566 no effect on the bank erosion rate as bespoke experiments demonstrate. The combined effects
567 result in a narrower, confined estuary planform, but with similar bar patterns and dynamics,
568 although higher in elevation, compared to the experiment without cohesive material reported
569 here [*Braat et al.*, 2018].

570 Nevertheless, the general evolution of the experiment can be compared to the Western Scheldt,
571 which evolved in the past 2700 years from a narrow creek in a peat bog to an alluvial estuary
572 with a quasi-periodic planform (Figure 11). The timescale over which estuaries widen from a
573 narrow creek after ingressions is typically in the order of hundreds of years, which may still be
574 an estimate on the higher end for organic peat, which decays rapidly after erosion [*Pierik et al.*,
575 2017; *de Haas et al.*, 2017] and thus does not contribute to sediment available for bar formation.
576 Despite their contrasting early evolution, the later stages of the experiment and natural systems
577 were more similar.

580 Bar dynamics typically occurs in tidal inlets, embayments and estuaries on timescales from
581 15-40 years [*Israel and Dunsbergen*, 1999; *Levoy et al.*, 2017]. A comparison of the experiment
582 with this timescale may be more appropriate, because these processes are not limited in
583 sediment supply. Nevertheless, scaling relations for bar patterns in experiments [*Kleinhans et al.*,
584 2015a] and the natural processes that form bars [*Leuven et al.*, 2016] and confine estuaries are
585 not well understood. Recent numerical models show that mud deposits may be required to
586 confine estuary planform and that self-formed estuaries with mud can reach an equilibrium
587 within 500-1000 years [*Braat et al.*, 2017].

4.3 Role of circulation cells and confluences on the evolution of estuaries

The historic evolution of channel and bar patterns in the Western Scheldt (1800-1900) was characterised by an initial phase of migration and meandering of the main ebb channels, after which the meander bends reached the embankments on the sides [Jeuken, 2000]. In the inner bends, the compound bars extended laterally and flood barbs formed. This evolution is very similar to the initial phases of the experiment (Figures 6,11). However, after 1900, the morphological evolution was largely influenced by human interference: dikes were constructed, side branches that slowly filled-in were embanked and the first dredging activities started in 1922 [Kleinjan, 1938; Jeuken, 2000].

In 1944, *van Veen*, described the occurrence of circulation patterns in the Western Scheldt, where flow circulates through an ebb and a flood channel enclosing an intertidal bar. These circulation cells are similar to the circulation cells observed in the experiment, where the main meandering channel is ebb dominated and circulation cells covered the flood barb and adjacent ebb channel. These circulation cells divide the Western Scheldt into six main zones, which were later described as macrocells [Winterwerp *et al.*, 2001; Toffolon and Crosato, 2007; Jeuken and Wang, 2010; Monge-Ganuzas *et al.*, 2013] (Supplementary Figure 6). These cells were determined from the observed morphology of the main ebb and flood tidal channels and numerically modelled residual flow, which resulted in cells that covered the enclosed area of an intertidal compound bar with its surrounding meandering channel. The boundaries of these cells in along-channel direction were chosen at the location of major channel confluences and correspond to the locations where the estuary width is relatively narrow. The concept of macrocells [e.g. Winterwerp *et al.*, 2001; Toffolon and Crosato, 2007; Jeuken and Wang, 2010; Monge-Ganuzas *et al.*, 2013] is similar to concept of mutually evasive transport paths [e.g. Ludwick, 1975; Harris, 1988; Dalrymple *et al.*, 1990; Wells, 1995; Harris *et al.*, 2004; Dalrymple and Choi, 2007]. The latter, for example, occurs around elongated tidal bars, where the opposite sides of the bar crest have opposing directions of residual sand transport and residual water flow, forming a circulation pattern. The difference between the latter and former group of authors is that the macrocells describe only the largest scale of bars, whereas the mutually evasive transport paths occur at a range of scales, including that of the smallest shoals as also observed in experiments [Kleinhans *et al.*, 2014, 2015b].

The experimental results in this study show that already after 800 tidal cycles serial circulation cells have evolved and that these circulation patterns can be used to explain how forced mid-channel bars cause bank erosion (Figure 7a,b). After the experimental estuary became wide enough, a pattern with parallel circulation cells or cells with a mixed coupling [Winterwerp *et al.*, 2001] evolved (Figure 7c,e). Later phases of the experiment illustrated that the boundary of two successive circulation cells typically occurred at a major confluence and at locations where the estuary width is relatively narrow. The length of circulation cells scales with bar length, and both bar length and circulation cell length correlate with estuary width (Figure 10b,c,d). These patterns resemble the patterns observed in the Western Scheldt (Figure 12, Supplementary Figure 6).

4.4 Cyclicity of channels and bars in tidal systems

Cyclicity is the periodic migration of channels and bars, in which the original configuration after a given period reoccurs. This has previously been reported for natural tidal systems as well as experiments. For example, experiments of short tidal basins show periodic migration of channels and shoals, which is coupled to reorganisation of the channels in the tidal basin [Kleinhans *et al.*, 2015b]. Most of the studies so far focussed on cyclicity on the ebb-tidal delta [e.g. Oost, 1995; Israel and Dunsbergen, 1999; Elias and van der Spek, 2006], on which channels migrate from one side to the other, after which they disappear and reappear at their initial position. However, besides ebb deltas and the quasi-cyclic morphologic behaviour of the smaller-scale connecting channels that link the large ebb and flood channels in macro-cells [van Veen, 1950; van den Berg *et al.*, 1996; Jeuken, 2000; Toffolon and Crosato, 2007; Swinkels *et al.*,

657 2009; *de Vriend et al.*, 2011], little is known about the cyclicity of bars and channels within tidal
658 basins or estuaries.

659 *Levoy et al.* [2017] observed an 18.6-year cycle in the migration of channels and tidal flats in the
660 bay of Mont-Saint-Michel (France). They state that the periodic increase and decrease in
661 flood-dominance corresponds with the periodic shift in the location of the channel, which is
662 either located in the north or the south of the embayment. In this case, the bayward migration
663 of tidal sand ridges forced a change in the in- and outflow direction of the tidal channels. It is
664 hypothesised that a progressively northward swing of the northern channel configuration is
665 caused by sand choking, i.e. a large sediment supply partly blocking the main channel. This
666 latter mechanism could be similar to the observations in the final stage of the scale-experiments,
667 in which the ebb-tidal delta progressively expands in landward direction, followed by a
668 southward migration of the channel at 11-12 m (Supplementary Figure 2s-u).

669 While not explicitly stated in the original paper [*Levoy et al.*, 2017], the presence of a monastery
670 and some local bedrock in the middle of the entrance of the embayment may have had a forcing
671 effect on the inflow location and direction of the tidal channels. Similarly, the local confinement
672 present eastward in the embayment could force the main confluence location there. The
673 observation in our experiments, where major confluences and narrow zones in the outline are
674 self-formed thus fits with observations in this natural system. In addition, *Levoy et al.* [2017]
675 recorded that infill of channels by reworking of bar sediments can cause sudden shifts of
676 channels, which was also observed in the experiments when an ebb channel progressively blocks
677 the evading flood channel by forming a u-shaped bar into that channel.

678 Our experimental results suggest that without any human interference (e.g. dredging or bank
679 protection) the morphodynamics of macrocells remain active: the roles and locations of ebb and
680 flood tidal channels may reverse within approximately 1000 tidal cycles and intertidal bars
681 between these channels are continuously reworked. This is in contrast with natural systems
682 under human interferences, in which dredging may cause degeneration of the affected cell and
683 subsequently evolve into a single-channel system [*Wang and Winterwerp*, 2001; *Jeuken and*
684 *Wang*, 2010; *Wang et al.*, 2015] and for which smaller connecting channels are disappearing by
685 marsh formation on top of the shoals [*Swinkels et al.*, 2009]. Open questions include what the
686 effect of dredging and dumping will be on the morphodynamics of estuaries and how an
687 engineered estuary compares to a reference case with exactly the same initial and boundary
688 conditions but without any human interference.

689 5 Conclusions

690 An experiment in a periodic tilting flume revealed the long-term evolution of channel and bar
691 patterns in self-formed estuaries. Typically, in the landward part a stable meandering channel
692 forms, whereas in the seaward part dynamic channels and bars form that periodically shift
693 laterally. The estuary banks are eroded in phases when forced mid-channel bars are present,
694 which results in an estuary planform that is locally wider than the ideal converging shape.
695 Zones with abundant and dynamic bars are separated by locations of channel confluences. We
696 conclude that stable confluence locations in self-formed estuaries are controlled by the spacing
697 of tidal bars, which both are a function of estuary width. The channels between the stable
698 confluences are highly dynamic, which results in a quasi-periodic estuary planform.

699 The self-formed experimental estuary specifically shows that major confluences occur at
700 relatively narrow parts in the outline and that these confinements are self-formed by sidebar
701 formation. This corresponds to observations in natural systems in which major confluences also
702 occur at self-formed confinements, for example by salt marsh formation, as well as at forced
703 confinements, for example by inherited geology or human engineering. However, natural
704 channels and bars are limited in their dynamics, because channels are largely fixed or
705 maintained in place. While the ideal estuary shape may be applicable to tidal creeks and
706 branches of deltas in equilibrium, the experimental results and observations in natural systems

707 suggest that in self-formed alluvial estuaries in absence of any external forcing (geology, human
708 influence) an autogenically-formed quasi-periodic estuary planform evolves.

709 Acknowledgments

710 This research was supported by the Dutch Technology Foundation TTW (grant Vici
711 016.140.316/13710 to MGK, which is part of the Netherlands Organisation for Scientific
712 Research (NWO, and is partly funded by the Ministry of Economic Affairs). This work is part
713 of the PhD research of JRFWL and LB. Detailed reviews by Bob Dalrymple, one anonymous
714 reviewer and steer by the editor and associate editor helped to improve the manuscript. We are
715 grateful for technical support by Marcel van Maarseveen, Chris Roosendaal, Henk Markies and
716 Arjan van Eijk. The authors contributed in the following proportions to conception and design,
717 data collection and processing, analysis and conclusions, and manuscript preparation:
718 JRFWL(55,45,75,75%), LB(5,45,0,0%), WMvD(5,5,10,10%), TdH(5,5,5,5%),
719 MGK(30,0,10,10%). EPvO conducted scaled gravity wave experiments in the Metronome and
720 analysed the resulting data as part of his MSc research and BGR contributed to conception and
721 design of the wave scaling. The data used are listed in the references, figures and supplements.

722 References

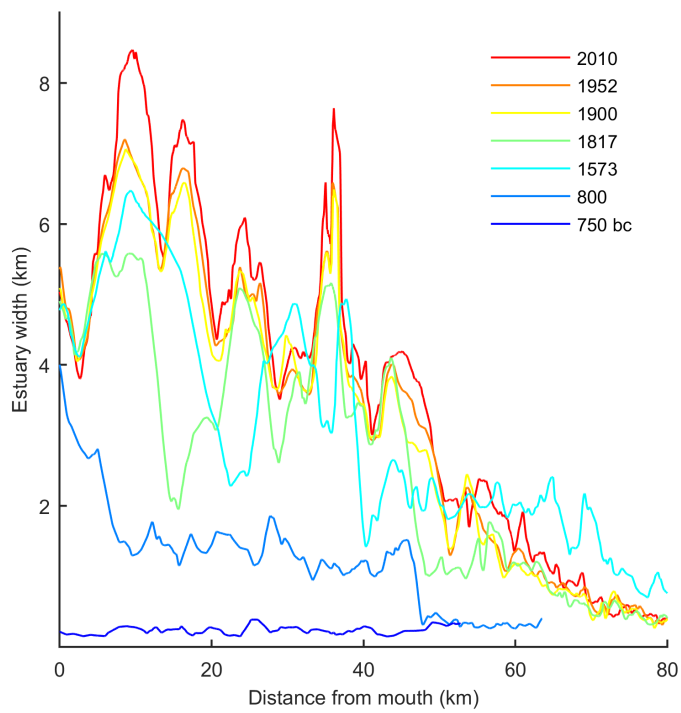
- 723 Agisoft, L. (2017), Agisoft photscan.
- 724 Ashmore, P. E. (2001), *Gravel-Bed River V*, chap. Braiding Phenomena: Statics and Kinetics,
725 pp. 95–114, New Zealand Hydrological Society Inc., Wellington, New Zealand.
- 726 Ashworth, P. J., J. L. Best, J. E. Roden, C. S. Bristow, and G. J. Klaassen (2000),
727 Morphological evolution and dynamics of a large, sand braid-bar, jamuna river, bangladesh,
728 *Sedimentology*, 47(3), 533–555.
- 729 Baar, A., J. de Smit, W. Uijtewaai, and M. Kleinhans (2018), Sediment transport of fine sand to
730 fine gravel on transverse bed slopes in rotating annular flume experiments [under review],
731 *Water Resources Research*, 54(1), 19–45, doi:10.1002/2017WR020604.
- 732 Bartels, P. (2015), Ups-and-downs of tidal systems: formation and development of ebb-and flood
733 tidal channels and bars., Master's thesis, Utrecht University.
- 734 Braat, L., T. van Kessel, J. R. F. W. Leuven, and M. G. Kleinhans (2017), Effects of mud
735 supply on large-scale estuary morphology and development over centuries to millennia, *Earth*
736 *Surface Dynamics*, 5, 617–652, doi:10.5194/esurf-5-617-2017.
- 737 Braat, L., J. R. F. W. Leuven, I. R. Lokhorst, and M. G. Kleinhans (2018), Effects of estuarine
738 mudflat formation on tidal prism and large-scale morphology in experiments, *Earth Surface*
739 *Processes and Landforms*, (revision submitted), doi:10.31223/osf.io/6y9n8.
- 740 Bridge, J. (2003), *Rivers and Floodplains*, 491 pp, Blackwell Publishing, Malden, Mass.
- 741 Chandler, J. H., K. Shiono, P. Rameshwaren, and S. N. Lane (2001), Measuring flume surfaces
742 for hydraulics research using a kodak dcs460, *The Photogrammetric Record*, 17(97), 39–61.
- 743 Cleveringa, J. (2013), Ontwikkeling mesoschaal westerschelde - instandhouding vaarpassen
744 schelde milieuvergunningen terugstorten baggerspecie (in dutch), *Tech. rep.*, ARCADIS.
- 745 Dalrymple, R. W., and K. Choi (2007), Morphologic and facies trends through the
746 fluvial–marine transition in tide-dominated depositional systems: a schematic framework for
747 environmental and sequence-stratigraphic interpretation, *Earth-Science Reviews*, 81(3),
748 135–174, doi:10.1016/j.earscirev.2006.10.002.
- 749 Dalrymple, R. W., and R. N. Rhodes (1995), Estuarine dunes and bars, *Geomorphology and*
750 *sedimentology of estuaries*, 53, 359–422.
- 751 Dalrymple, R. W., R. Knight, B. A. Zaitlin, and G. V. Middleton (1990), Dynamics and facies
752 model of a macrotidal sand-bar complex, cobequid bay–salmon river estuary (bay of fundy),
753 *Sedimentology*, 37(4), 577–612.
- 754 Dalrymple, R. W., B. A. Zaitlin, and R. Boyd (1992), Estuarine facies models: conceptual basis
755 and stratigraphic implications: perspective, *Journal of Sedimentary Research*, 62(6),
756 doi:10.1306/D4267A69-2B26-11D7-8648000102C1865D.

- 757 Davis Jr, R. A., and M. O. Hayes (1984), What is a wave-dominated coast?, *Marine geology*,
758 60(1-4), 313–329, doi:10.1016/0025-3227(84)90155-5.
- 759 de Haas, T., H. Pierik, A. van der Spek, K. Cohen, B. van Maanen, and M. Kleinans (2017),
760 Holocene evolution of tidal systems in the netherlands: Effects of rivers, coastal boundary
761 conditions, eco-engineering species, inherited relief and human interference, *Earth-Science*
762 *Reviews*, 177, 139 – 163, doi:10.1016/j.earscirev.2017.10.006.
- 763 de Vriend, H. J., Z. B. Wang, T. Ysebaert, P. M. Herman, and P. Ding (2011),
764 Eco-morphological problems in the yangtze estuary and the western scheldt, *Wetlands*, 31(6),
765 1033–1042, doi:10.1007/s13157-011-0239-7.
- 766 Eke, E. (2014), Numerical modeling of river migration incorporating erosional and depositional
767 bank processes, Ph.D. thesis, University of Illinois at Urbana-Champaign.
- 768 Elias, E. P., and A. J. van der Spek (2006), Long-term morphodynamic evolution of texel inlet
769 and its ebb-tidal delta (the netherlands), *Marine Geology*, 225(1), 5–21.
- 770 Elias, E. P., A. J. van der Spek, and M. Lazar (2017), The ŚvoordeltaŠ, the contiguous ebb-tidal
771 deltas in the sw netherlands: large-scale morphological changes and sediment budget
772 1965–2013; impacts of large-scale engineering, *Netherlands Journal of Geosciences*, 96(3),
773 233–259.
- 774 Fonstad, M. A., J. T. Dietrich, B. C. Courville, J. L. Jensen, and P. E. Carbonneau (2013),
775 Topographic structure from motion: a new development in photogrammetric measurement,
776 *Earth Surface Processes and Landforms*, 38(4), 421–430.
- 777 Harris, P. T. (1988), Large-scale bedforms as indicators of mutually evasive sand transport and
778 the sequential infilling of wide-mouthed estuaries, *Sedimentary Geology*, 57(3-4), 273–298.
- 779 Harris, P. T., M. G. Hughes, E. K. Baker, R. W. Dalrymple, and J. B. Keene (2004), Sediment
780 transport in distributary channels and its export to the pro-deltaic environment in a tidally
781 dominated delta: Fly river, papua new guinea, *Continental Shelf Research*, 24(19), 2431–2454.
- 782 Hijma, M. P., and K. M. Cohen (2011), Holocene transgression of the rhine river mouth area,
783 the netherlands/southern north sea: palaeogeography and sequence stratigraphy,
784 *Sedimentology*, 58(6), 1453–1485.
- 785 Hundey, E., and P. Ashmore (2009), Length scale of braided river morphology, *Water Resources*
786 *Research*, 45(8).
- 787 Ikeda, S., and G. Parker (1989), *River Meandering*, American Geophysical Union.
- 788 Israel, C., and D. Dunsbergen (1999), Cyclic morphological development of the ameland inlet,
789 the netherlands, in *Proceedings of Symposium on River, Coastal and Estuarine*
790 *Morphodynamics (Genova, Italy)*, vol. 2, pp. 705–714.
- 791 Jeuken, M., and Z. Wang (2010), Impact of dredging and dumping on the stability of ebb–flood
792 channel systems, *Coastal Engineering*, 57(6), 553–566.
- 793 Jeuken, M.-C. J. L. (2000), *On the morphologic behaviour of tidal channels in the Westerschelde*
794 *estuary*, Utrecht University.
- 795 Kleinans, M., T. Van Rosmalen, C. Roosendaal, M. van der Vegt, et al. (2014), Turning the
796 tide: mutually evasive ebb-and flood-dominant channels and bars in an experimental estuary,
797 *Advances in Geosciences*, 39, 21–26.
- 798 Kleinans, M. G., and J. H. van den Berg (2011), River channel and bar patterns explained and
799 predicted by an empirical and a physics-based method, *Earth Surface Processes and*
800 *Landforms*, 36(6), 721–738, doi:10.1002/esp.2090.
- 801 Kleinans, M. G., C. Braudrick, W. M. Van Dijk, W. I. Van de Lageweg, R. Teske, and
802 M. Van Oorschot (2015a), Swiftness of biomorphodynamics in lilliput-to giant-sized rivers
803 and deltas, *Geomorphology*, 244, 56–73.
- 804 Kleinans, M. G., R. T. Scheltinga, M. Vegt, and H. Markies (2015b), Turning the tide: growth
805 and dynamics of a tidal basin and inlet in experiments, *Journal of Geophysical Research:*
806 *Earth Surface*, 120(1), 95–119.
- 807 Kleinans, M. G., M. van der Vegt, J. Leuven, L. Braat, H. Markies, A. Simmelink,
808 C. Roosendaal, A. van Eijk, P. Vrijbergen, and M. van Maarseveen (2017a), Turning the tide:
809 comparison of tidal flow by periodic sealevel fluctuation and by periodic bed tilting in the
810 metronome tidal facility, *Earth Surface Dynamics Discussions*, 2017, 1–35,

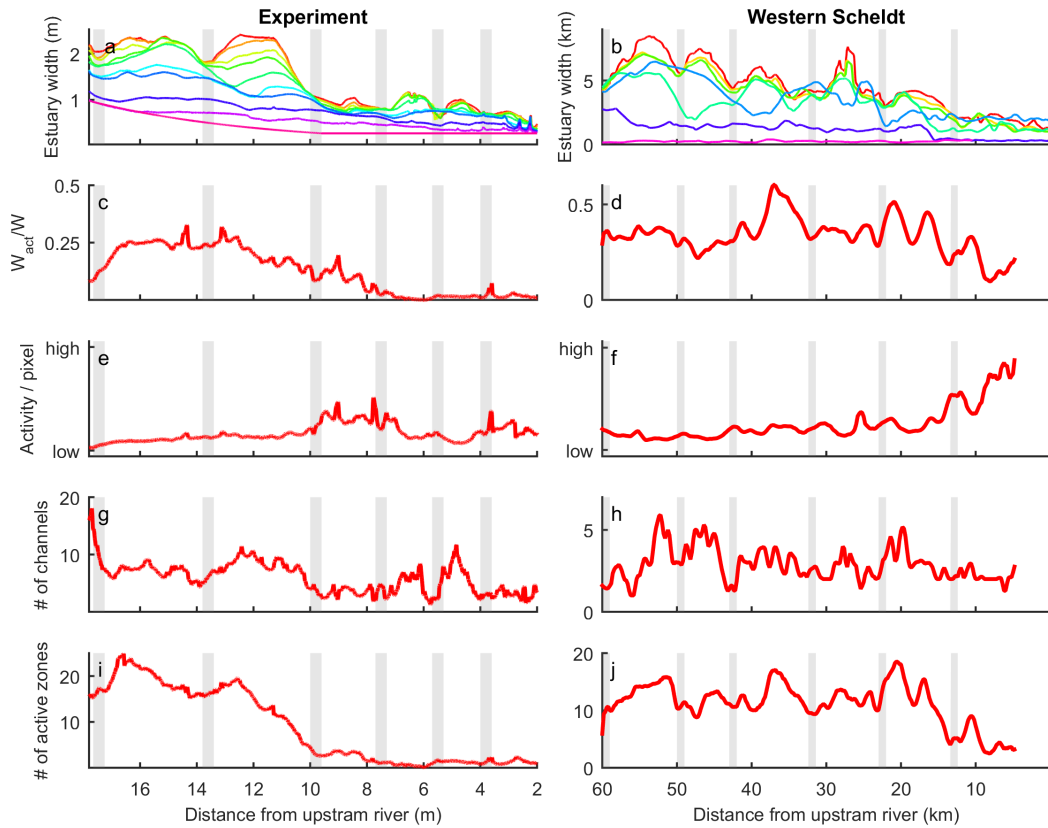
- 811 doi:10.5194/esurf-2017-11.
- 812 Kleinhans, M. G., J. R. Leuven, L. Braat, and A. Baar (2017b), Scour holes and ripples occur
813 below the hydraulic smooth to rough transition of movable beds, *Sedimentology*.
- 814 Kleinjan, I. (1938), Het gebied van de westerschelde nabij bath, *Rapport R88a, 88b, 88c*.
815 *Rijkswaterstaat, Dordrecht*.
- 816 Lane, S., K. Richards, and J. Chandler (1993), Developments in photogrammetry; the
817 geomorphological potential, *Progress in Physical Geography*, 17(3), 306–328.
- 818 Langbein, W. (1963), The hydraulic geometry of a shallow estuary, *Hydrological Sciences*
819 *Journal*, 8(3), 84–94, doi:10.1080/02626666309493340.
- 820 Lanzoni, S., and G. Seminara (2006), On the nature of meander instability, *Journal of*
821 *Geophysical Research: Earth Surface*, 111(F4), doi:10.1029/2005JF000416.
- 822 Leopold, L. B., and M. G. Wolman (1960), River meanders, *Geological Society of America*
823 *Bulletin*, 71(6), 769–793.
- 824 Leuven, J. (2014), Turning the tide: The effect of river discharge on estuary dynamics and
825 equilibrium, Master's thesis, Utrecht University.
- 826 Leuven, J. R. F. W., M. G. Kleinhans, S. A. H. Weisscher, and M. van der Vegt (2016), Tidal
827 sand bar dimensions and shapes in estuaries, *Earth-science reviews*, 161, 204–233,
828 doi:10.1016/j.earscirev.2016.08.004.
- 829 Leuven, J. R. F. W., T. Haas, L. Braat, and M. G. Kleinhans (2018a), Topographic forcing of
830 tidal sand bar patterns for irregular estuary planforms, *Earth Surface Processes and*
831 *Landforms*, 43, 172–186, doi:10.1002/esp.4166.
- 832 Leuven, J. R. F. W., S. Selaković, and M. G. Kleinhans (2018b), Morphology of bar-built
833 estuaries: empirical relation between planform shape and depth distribution, *Earth Surface*
834 *Dynamics*, (in press), 1–24, doi:10.5194/esurf-2018-18.
- 835 Leuven, J. R. F. W., B. van Maanen, B. R. Lexmond, B. V. van der Hoek, M. J. Spruijt, and
836 M. G. Kleinhans (2018c), Dimensions of fluvial-tidal meanders: Are they disproportionately
837 large?, *Geology*, (in press).
- 838 Levoy, F., E. Anthony, J. Dronkers, O. Monfort, G. Izabel, and C. Larsonneur (2017), Influence
839 of the 18.6-year lunar nodal tidal cycle on tidal flats: Mont-saint-michel bay, france, *Marine*
840 *Geology*, 387, 108–113.
- 841 Lokhorst, I., L. Braat, J. R. F. W. Leuven, A. W. Baar, M. van Oorschot, S. Selaković, and
842 M. G. Kleinhans (2018), Morphological effects of vegetation on the fluvial-tidal transition in
843 holocene estuaries, *Earth Surface Dynamics Discussions*, 2018, 1–28,
844 doi:10.5194/esurf-2018-29.
- 845 Ludwick, J. C. (1975), Tidal currents, sediment transport, and sand banks in chesapeake bay
846 entrance, virginia, in *Geology and Engineering*, pp. 365–380, Elsevier,
847 doi:10.1016/B978-0-12-197502-9.50027-7.
- 848 Manning, A. (2007), Enhanced uk estuaries database: explanatory notes and metadata, *Tech.*
849 *Rep. TR167*, HR Wallingford Tech. Report, TR167, UK.
- 850 Mayor-Mora, R. E. (1977), Laboratory investigation of tidal inlets on sandy coasts., *Tech. rep.*,
851 DTIC Document.
- 852 Monge-Ganuzas, M., A. Cearreta, and G. Evans (2013), Morphodynamic consequences of
853 dredging and dumping activities along the lower oka estuary (urdaibai biosphere reserve,
854 southeastern bay of biscay, spain), *Ocean & coastal management*, 77, 40–49.
- 855 Morgan, J. A., D. J. Brogan, and P. A. Nelson (2017), Application of structure-from-motion
856 photogrammetry in laboratory flumes, *Geomorphology*, 276, 125–143.
- 857 Mori, N., and K.-A. Chang (2003), Experimental study of a horizontal jet in a wavy
858 environment, *Journal of engineering mechanics*, 129(10), 1149–1155.
- 859 Oost, A. P. (1995), Dynamics and sedimentary developments of the dutch wadden sea with a
860 special emphasis on the frisian inlet: a study of the barrier islands, ebb-tidal deltas, inlets and
861 drainage basins, Ph.D. thesis, Utrecht University.
- 862 Parker, G., Y. Shimizu, G. Wilkerson, E. C. Eke, J. D. Abad, J. Lauer, C. Paola, W. E. Dietrich,
863 and V. Voller (2011), A new framework for modeling the migration of meandering rivers,
864 *Earth Surface Processes and Landforms*, 36(1), 70–86, doi:10.1002/esp.2113.

- 865 Pierik, H., K. Cohen, P. Vos, A. van der Spek, and E. Stouthamer (2017), Late holocene
866 coastal-plain evolution of the netherlands: the role of natural preconditions in human-induced
867 sea ingressions, *Proceedings of the Geologists' Association*, 128(2), 180–197.
- 868 Pillsbury, G. (1956), Tidal hydraulics. revised edition, corps of engineers, *US Army, May*.
- 869 Repetto, R., and M. Tubino (2001), Topographic expressions of bars in channels with variable
870 width, *Physics and Chemistry of the Earth, Part B: Hydrology, Oceans and Atmosphere*, 26(1),
871 71–76.
- 872 Reynolds, O. (1887), On certain laws relating to the regime of rivers and on the possibility of
873 experiments at small scale, *Brit. Ass. Report*.
- 874 Reynolds, O. (1889), On model estuaries in report of the committee appointed to investigate the
875 action of waves and currents on the beds and fore shores of estuaries by means of working
876 models, *Rept. Brit. Assoc.* pp. 327–343.
- 877 Savenije, H. H. (2015), Prediction in ungauged estuaries: an integrated theory, *Water Resources
878 Research*, 51(4), 2464–2476, doi:10.1002/2015WR016936.
- 879 Schuurman, F., and M. G. Kleinhans (2015), Bar dynamics and bifurcation evolution in a
880 modelled braided sand-bed river, *Earth Surface Processes and Landforms*, 40(10), 1318–1333.
- 881 Schuurman, F., W. A. Marra, and M. G. Kleinhans (2013), Physics-based modeling of large
882 braided sand-bed rivers: Bar pattern formation, dynamics, and sensitivity, *Journal of
883 geophysical research: Earth Surface*, 118(4), 2509–2527.
- 884 Schuurman, F., Y. Shimizu, T. Iwasaki, and M. Kleinhans (2016), Dynamic meandering in
885 response to upstream perturbations and floodplain formation, *Geomorphology*, 253, 94–109.
- 886 Schuurman, F., W. Ta, S. Post, M. Sokolewicz, M. Busnelli, and M. Kleinhans (2018), Response
887 of braiding channel morphodynamics to peak discharge changes in the upper yellow river,
888 *Earth Surface Processes and Landforms*, doi:doi.org/10.1002/esp.4344.
- 889 Seminara, G. (2010), Fluvial sedimentary patterns, *Annual Review of Fluid Mechanics*, 42,
890 43–66.
- 891 Stefanon, L., L. Carniello, A. D'Alpaos, and S. Lanzoni (2010), Experimental analysis of tidal
892 network growth and development, *Continental Shelf Research*, 30(8), 950–962.
- 893 Struiksmā, N., K. Olesen, C. Flokstra, and H. De Vriend (1985), Bed deformation in curved
894 alluvial channels, *Journal of Hydraulic Research*, 23(1), 57–79.
- 895 Swinkels, C. M., C. M. Jeuken, Z. B. Wang, and R. J. Nicholls (2009), Presence of connecting
896 channels in the western scheldt estuary, *Journal of Coastal Research*, pp. 627–640.
- 897 Tambroni, N., M. Bolla Pittaluga, and G. Seminara (2005), Laboratory observations of the
898 morphodynamic evolution of tidal channels and tidal inlets, *Journal of Geophysical Research:
899 Earth Surface*, 110(F4).
- 900 Tambroni, N., R. Luchi, and G. Seminara (2017), Can tide dominance be inferred from the point
901 bar pattern of tidal meandering channels?, *Journal of Geophysical Research: Earth Surface*,
902 122(2), 492–512, doi:10.1002/2016JF004139.
- 903 Toffolon, M., and A. Crosato (2007), Developing macroscale indicators for estuarine
904 morphology: The case of the scheldt estuary, *Journal of Coastal Research*, 23(1), 195–212.
- 905 Townend, I. (2012), The estimation of estuary dimensions using a simplified form model and
906 the exogenous controls, *Earth Surface Processes and Landforms*, 37(15), 1573–1583,
907 doi:10.1002/esp.3256.
- 908 Tubino, M., R. Repetto, and G. Zolezzi (1999), Free bars in rivers, *Journal of Hydraulic
909 Research*, 37(6), 759–775.
- 910 van de Lageweg, W. I., W. M. van Dijk, A. W. Baar, J. Rutten, and M. G. Kleinhans (2014),
911 Bank pull or bar push: What drives scroll-bar formation in meandering rivers?, *Geology*,
912 42(4), 319–322.
- 913 van den Berg, J. H., C. J. Jeuken, and A. J. Van der Spek (1996), Hydraulic processes affecting
914 the morphology and evolution of the westerschelde estuary, in *Estuarine Shores: Evolution,
915 Environments and Human Alterations*, edited by K. F. Nordstrom and C. T. Roman, pp.
916 157–184, John Wiley & Sons Ltd.
- 917 van der Spek, A. J., and D. J. Beets (1992), Mid-holocene evolution of a tidal basin in the
918 western netherlands: a model for future changes in the northern netherlands under conditions

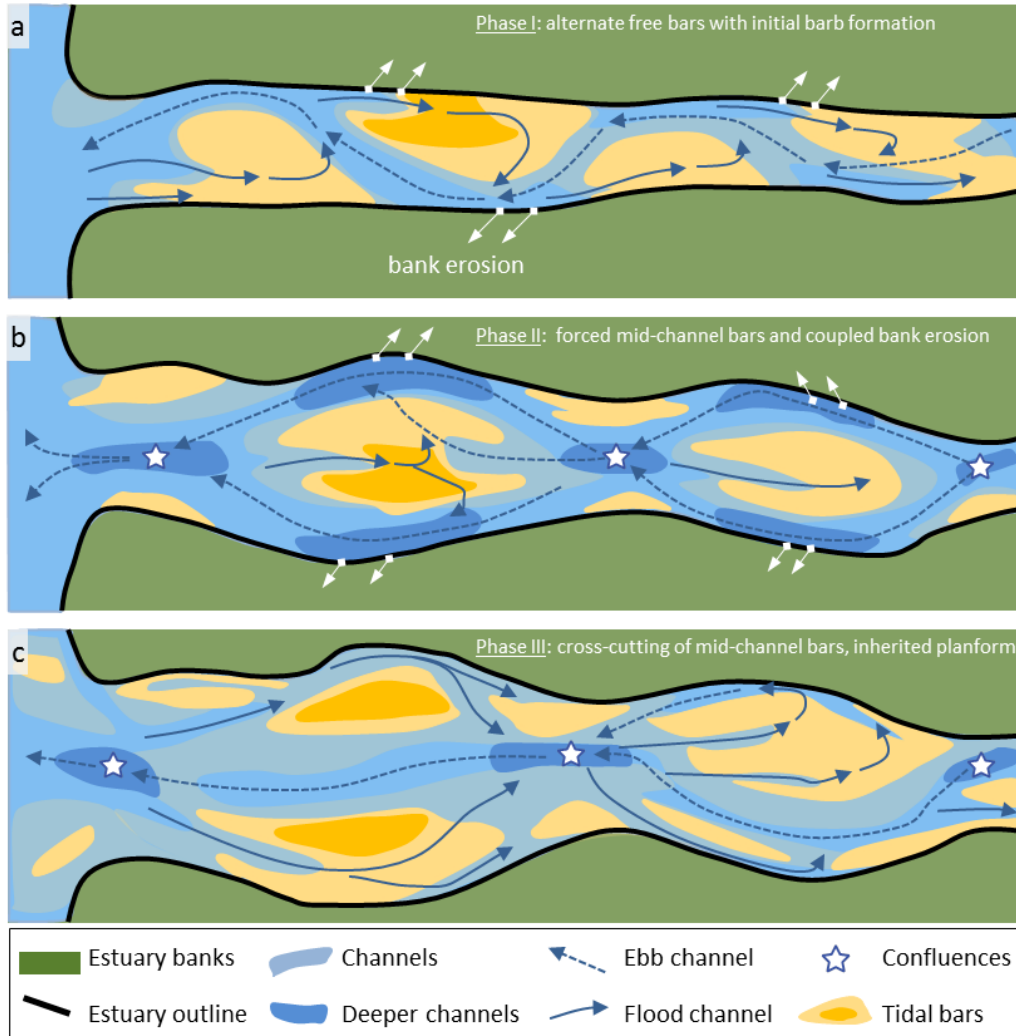
- of accelerated sea-level rise?, *Sedimentary geology*, 80(3), 185–197.
- van der Wegen, M., and J. Roelvink (2012), Reproduction of estuarine bathymetry by means of a process-based model: Western scheldt case study, the netherlands, *Geomorphology*, 179, 152–167, doi:10.1016/j.geomorph.2012.08.007.
- van Dijk, W. M., W. I. van de Lageweg, and M. G. Kleinhans (2012), Experimental meandering river with chute cutoffs, *Journal of Geophysical Research: Earth Surface*, 117(F3), n/a–n/a, doi:10.1029/2011JF002314, f03023.
- van Dijk, W. M., W. I. Lageweg, and M. G. Kleinhans (2013), Formation of a cohesive floodplain in a dynamic experimental meandering river, *Earth Surface Processes and Landforms*, 38(13), 1550–1565.
- van Veen, J. (1944), Schelderegiem en schelderegie, *Tech. rep.*, Rijkswaterstaat reprint 1993, Middelburg.
- van Veen, J. (1950), Eb-en vloedschaarsystemen in de nederlandse getijwateren, *Tijdschrift Koninklijk Nederlands Aardrijkskundig Genootschap*, 67, 303–325.
- Vlaswinkel, B. M., and A. Cantelli (2011), Geometric characteristics and evolution of a tidal channel network in experimental setting, *Earth Surface Processes and Landforms*, 36(6), 739–752.
- Wang, Z., and J. Winterwerp (2001), Impact of dredging and dumping on the stability of ebb-flood channel systems, in *Proceedings of the 2nd IAHR symposium on River, Coastal and Estuarine Morphodynamics*, pp. 515–524.
- Wang, Z., D. Van Maren, P. Ding, S. Yang, B. Van Prooijen, P. De Vet, J. Winterwerp, H. De Vriend, M. Stive, and Q. He (2015), Human impacts on morphodynamic thresholds in estuarine systems, *Continental Shelf Research*, 111, 174–183.
- Wells, J. T. (1995), Tide-dominated estuaries and tidal rivers, in *Developments in Sedimentology*, vol. 53, pp. 179–205, Elsevier, doi:10.1016/S0070-4571(05)80026-3.
- Westoby, M., J. Brasington, N. Glasser, M. Hambrey, and J. Reynolds (2012), Structure-from-motion photogrammetry: A low-cost, effective tool for geoscience applications, *Geomorphology*, 179, 300–314.
- Winterwerp, J., Z. Wang, M. Stive, A. Arends, C. Jeuken, C. Kuijper, and P. Thoolen (2001), A new morphological schematization of the western scheldt estuary, the netherlands, in *Proceedings of the 2nd IAHR symposium on River, Coastal and Estuarine Morphodynamics*, pp. 525–533.
- Wu, F.-C., Y.-C. Shao, and Y.-C. Chen (2011), Quantifying the forcing effect of channel width variations on free bars: Morphodynamic modeling based on characteristic dissipative galerkin scheme, *Journal of Geophysical Research: Earth Surface*, 116(F3).
- Yalin, M. (1971), On the formation of dunes and meanders, in *Proceedings of the 14th Congress of the International Association for Hydraulic Research*, vol. 3, pp. 101–108.
- Zolezzi, G., R. Luchi, and M. Tubino (2012), Modeling morphodynamic processes in meandering rivers with spatial width variations, *Reviews of Geophysics*, 50(4), doi:10.1029/2012RG000392.



578 **Figure 11.** The estuary width profile of the Western Scheldt (The Netherlands) over time, which shows a
579 similar evolution as the experiment.



628 **Figure 12.** Along-channel profiles of (a,b) local estuary width over time, (c,d) time-averaged active channel
 629 width normalised with local estuary width, (e,f) sum of absolute bed level change per pixel, (g,h) number of
 630 channels in cross-section and (i,j) number of active areas in cross-section. Shading indicates locations of
 631 confinement in the estuary outline. These locations correspond with locations where the active width, activity
 632 per pixel and number of channels are generally low. The along-channel profiles (c-j) were averaged over the
 633 period 7500-15000 cycles for the experiment and the years 2000-2015 for the western Scheldt.



634 **Figure 13.** Conceptual model for the development of self-formed estuaries. (a) Phase I: the initial
 635 converging channel widens and (free) migrating alternate bars form. The meandering channel around the
 636 alternate bars is predominantly used as ebb channel, eroding the outer bends. While the alternate bars widen,
 637 initial flood barbs form onto the alternate bars. The main meandering channel migrates slightly seaward in
 638 Phase I, causing a longitudinal displacement in the next phase. (b) Phase II: the flood barb channels
 639 progressively cut through the alternate bars, isolating forced mid-channel bars in the middle of the estuary.
 640 This creates two major confluences: one at the mouth and one upstream of the mid channel bar. The flow is
 641 diverted around the mid-channel bar, which causes bank erosion, resulting in an even more irregular planform.
 642 (c) Phase III: the barb channels on the mid-channel bar enlarge and subsequently connect, cross-cutting the
 643 bar. This forms a new channel in the middle of the estuary and limits the erosion of the estuary banks. The
 644 resulting quasi-periodic planform is inherited from phase II. Major confluences separate zones in which
 645 channels periodically rework tidal bars.